Journal of Manufacturing Systems 62 (2022) 145–163

Contents lists available at ScienceDirect

Journal of Manufacturing Systems

journal homepage: www.elsevier.com/locate/jmansys

Review

Machine learning for metal additive manufacturing: Towards a physics-informed data-driven paradigm

Shenghan Guo [a], Mohit Agarwal [b], Clayton Cooper [c], Qi Tian [d,e], Robert X. Gao [c], Weihong Guo Grace [e,f,*], Yuebin Guo [b,f]

[a] The School of Manufacturing Systems and Networks, Arizona State University, Mesa, AZ, 85212, USA
[b] Department of Mechanical and Aerospace Engineering, Rutgers University-New Brunswick, Piscataway, NJ, 08854, USA
[c] Department of Mechanical and Aerospace Engineering, Case Western Reserve University, Cleveland, OH, 44106, USA
[d] The State Key Laboratory of Coastal and Offshore Engineering, Dalian University of Technology, Dalian, 116024, China
[e] Department of Industrial and Systems Engineering, Rutgers University-New Brunswick, Piscataway, NJ, 08854, USA
[f] New Jersey Advanced Manufacturing Institute, Rutgers University-New Brunswick, Piscataway, NJ, 08854, USA

ARTICLE INFO

Keywords:
Machine learning
Deep learning
Additive manufacturing
Physics of manufacturing processes

ABSTRACT

Machine learning (ML) has shown to be an effective alternative to physical models for quality prediction and process optimization of metal additive manufacturing (AM). However, the inherent "black box" nature of ML techniques such as those represented by artificial neural networks has often presented a challenge to interpret ML outcomes in the framework of the complex thermodynamics that govern AM. While the practical benefits of ML provide an adequate justification, its utility as a reliable modeling tool is ultimately reliant on assured consistency with physical principles and model transparency. To facilitate the fundamental needs, physics-informed machine learning (PIML) has emerged as a hybrid machine learning paradigm that imbues ML models with physical domain knowledge such as thermomechanical laws and constraints. The distinguishing feature of PIML is the synergistic integration of data-driven methods that reflect system dynamics in real-time with the governing physics underlying AM. In this paper, the current state-of-the-art in metal AM is reviewed and opportunities for a paradigm shift to PIML are discussed, thereby identifying relevant future research directions.

1. Introduction

Additive manufacturing (AM) is well-recognized as a fast, flexible, and eco-friendly [1] technology for manufacturing metal parts. Metal AM processes, e.g., direct energy deposition (DED) and powder bed fusion (PBF), have been applied to aerospace, medicine, health care, and other fields [2] to produce high-value, customized products. Accompanying these industrial needs is a high standard for part quality, which requires effective monitoring of the metal AM processes to optimize process parameters such that the parts built will exhibit minimal defects and meet performance expectations. Toward this end, extensive efforts have been made in optimizing AM processes through modeling and simulations in a digital environment before experiments are conducted to minimize material costs associated with trial-and-error while maximizing process performance. These efforts can be categorized into two families: physics-based and data-driven methods.

Physics-based methods present process models that capture the physical principles underlying AM processes by using either analytical or numerical methods to emulate physical behavior at varying scales, e.g., atomic, microscale, or macroscopic. They are established either thermo-mechanically, based on process physics, or empirically through experimental findings. As a result, they can explain process mechanics and provide explicit insights into process phenomena, thereby providing guidance on minimizing AM process variabilities, part deficiencies, and improving overall process optimization [3,4]. However, due to model simplifications that are necessary to reduce model derivation complexity, physics-based models may be limited in comprehensively covering the entire spectrum of process variability. Specifically for physics-based models that are numerical and iterative in nature, e.g., finite element models, simulation has exponential time *and* memory complexity as a function of both the resolution and the number of elements to be simulated. As a result, this category of physical methods is infeasible for *in-situ* real-time usage and oftentimes impractical in the fast-paced development environment of industrial AM.

Data-driven methods such as machine learning (ML) algorithms are

* Corresponding author at: Department of Industrial and Systems Engineering, Rutgers University-New Brunswick, Piscataway, NJ, 08854, USA.
E-mail address: wg152@soe.rutgers.edu (W. Guo).

https://doi.org/10.1016/j.jmsy.2021.11.003
Received 23 August 2021; Received in revised form 5 November 2021; Accepted 6 November 2021
Available online 30 November 2021

Nomenclature

Ac	Accuracy
AM	Additive manufacturing
ANN	Artificial neural network
ASTM	American Society for Testing and Materials
CART	Classification and regression tree
CNN	Convolutional neural network
DBN	Deep belief network
DED	Directed energy deposition
EBAM	Electron beam additive manufacturing
EBM	Electron beam melting
EL	Elongation (failure strain)
f	Generalized ML model
F_1	F_1 score for classification
FEA	Finite element analysis
GAANFIS	Genetic algorithm adaptive NFI system
GD	Geometrical deviation
GDP	Geometric deviation prognosis
GMM	Gaussian mixture model
GPR	Gaussian process regression
HAGB	High-angle grain boundary
HIP	Hot isostatic pressing
KNN	K-nearest neighbors
LAGB	Low-angle grain boundary
LIME	Local interpretable model-agnostic explanations
LMD	Laser metal deposition
LRP	Layer-wise relevance propagation
MAPE	Mean absolute percentage error
ML	Machine learning
MLP	Multi-layer perceptron
MP	Microstructure prognosis
MPP	Melt pool prognosis
NFI	Neuro-fuzzy inference
PBF	Powder bed fusion
PIMA	Physics-informed model architecture
PIMC	Physics-informed model component
PIMI	Physics-informed model input
PIML	Physics-informed ML
PIMO	Physics-informed model output
PIMT	Physics-informed model training
PINN	Physics-informed neural network
PP	Porosity prognosis
Pr	Precision
Re	Recall
R^2	Coefficient of determination
RF	Random forest
RL	Reinforcement learning
RMSE	Root mean squared error
SHAP	Shapley additive explanations
SLA	Stereolithography
SLD	Sequential laser deposition
SLM	Selective laser melting
SLS	Selective laser sintering
SR	Surface roughness
SRP	Surface roughness prognosis
SS	Specific strength
SVM	Support vector machine
$\boldsymbol{w}$	Trainable parameters of f
UTS	Ultimate tensile stress
$\boldsymbol{x}_i$	ML model input instance i
$\boldsymbol{y}_i$	Ground truth value instance i
$\hat{\boldsymbol{y}}_i$	ML model output instance i
YM	Young's modulus
YS	Yield stress

capable of harnessing data of high dimensionality and heterogeneity and leveraging the full spectrum of process parameters beyond those incorporated in physical models. Complemented by sensing data measured during the AM process in real-time, such methods can effectively complement the physical understanding of the process by automatically and continually updating themselves through learning from the data and experience [5,6]. These characteristics imply several intrinsic advantages of ML as a means for metal AM process modeling and monitoring. First, ML models can be computationally efficient once properly trained [7], thus providing a good fit for analyzing dynamic thermomechanical phenomena [8] in metal AM processes. Second, ML methods do not pose restrictive assumptions on the processes being analyzed [9–11], and are thus adaptable to a broad range of process variability. Third, data-driven models are renewable and generalizable [12] as the basic structure of pretrained models can be retained and updated using new data before being transferred to other processes that are suited for analysis using the updated ML models [13,14]. Finally, ML can be leveraged to solve a wide variety of auxiliary problems in AM that are difficult to solve using traditional approaches, including cost estimation [15], manufacturability assessment [16,17], and closed-loop quality control [18].

The above advantages of data-driven models have been well-recognized by the research community [19], and considerable efforts have been made to leverage ML for metal AM studies. Examples include Khanzadeh et al. [20], Khanzadeh et al. [21], and Guo et al. [22] that analyzed *in-situ* thermal images of melt pools from DED with ML models and developed techniques for real-time prediction of porosity. Similarly, Shevchik et al. [23] and Wasmer et al. [24] demonstrated the feasibility of training ML-based quality prediction models with acoustic emissions from metal AM processes. Closed-loop control systems for metal AM were enabled by ML in Jafari-Marandi et al. [25], Liu et al. [26], and Renken et al. [27], which connected the design and printing/finishing stages in metal AM and achieved reverse process parameter optimization. These studies have facilitated improvements in quality and design for metal AM and expanded the scope of ML.

While the effectiveness of ML-based metal AM process modeling and control has been demonstrated, and more advances in ML-based methods are foreseeable [19], a major hurdle in the widespread acceptance of ML-based methods is their lack of physical interpretability. ML models' understanding of the underlying physics in metal AM is constrained by the physical meaningfulness of the input/output data as well as by the model architecture itself. Since datasets collected from diverse applications may not fully represent the complete AM process physics, how to intuitively enhance ML models' awareness of the underlying process physics toward full model interpretability has remained a challenge. Further challenges due to the lack of physical intuition in model construction include impractical model prediction results [28–30] and susceptibility to data pollution caused by noise, missing or incorrect data labels, etc.

An emerging topic in imbuing ML models with physical intuition is **Physics-Informed Machine Learning (PIML)**, which consists of hybrid methods that incorporate physical knowledge and domain constraints into ML to achieve interpretable model design, input, and output. Although still in its infancy at the current stage, the PIML paradigm has already attracted an increasing level of attention due to its potential for future exploration.

This paper presents a systematic review of the state-of-the-art in ML-based metal AM process modeling and control by summarizing common

methods developed in this field and revealing open questions and challenges. By highlighting of the potential of PIML, the review further aims to provide a roadmap to researchers in both the AM and ML communities for future synergy that enables PIML-driven, "smart" metal AM applications.

This paper distinguishes itself from other AM and ML review articles in the published literature [8,30–33] by providing the above-described roadmap and constitutes the first work in PIML for AM to guide the reader through the foundations of metal AM, identify outstanding challenges, and propose a comprehensive solution based on PIML. Additionally, the content of the paper establishes a foundation to further develop AM using physics, which is a research gap identified by previous works [8,30,31].

The rest of this paper is organized as follows. Section 2 briefly explains the mechanisms of metal AM and introduces major, representative AM processes. Section 3 reviews the state of ML-based metal AM process modeling and monitoring techniques. Section 4 introduces PIML as a potential enabler for higher level of effectiveness and efficiency in AM process modeling and control, followed by Section 5 where a vision for PIML-based metal AM is presented. Section 6 summarizes findings from the paper with a conclusion.

2. Metal additive manufacturing processes

The concept of modern AM originated in the early 1980s with the development of resin-based approaches. These included photo-hardening structural polymers in 1981 [34] and the advent of stereo-lithography (SLA) in 1984 [35]. A flurry of process variants soon followed, resulting in many unique metal AM processes being developed. To categorize metal AM processes as a whole, ASTM 52900:2015(E) [36] separates AM processes into seven categories. PBF and DED contain the majority of current metal AM research and therefore merit discussion in this paper. Table 1 presents a historical overview of metal AM development in these categories, which are discussed in detail in the following sections.

2.1. Powder bed fusion

PBF is an "additive manufacturing process in which thermal energy selectively fuses regions of a powder bed" [36]. By definition, PBF can be utilized for polymers, ceramics, and metals, though metal-based AM has become a dominant research thrust according to [44]. Between 1989 and 1995, three major PBF processes have emerged, with selective laser sintering (SLS) being the first PBF process to be patented and commercialized [38]. Subsequently, electron beam melting (EBM) [39] and selective laser melting (SLM) were developed [40]. These three techniques under PBF are notable because they laid a foundation for derivative PBF processes that would follow in the subsequent decades.

Fig. 1 shows a typical SLM setup where a powder deposition system places a 20−50 μm thick powder layer onto a build platform inside a build chamber. The chamber is filled with inert gas (e.g., argon) so that the metal does not oxidize during melting and re-solidification. A laser beam selectively melts the powder by following a toolpath generated from a CAD file of the part being produced. After the completion of one layer, the build platform will move downwards a distance equal to the thickness of one layer and a new layer of powder will be deposited. This cycle repeats itself until the whole part is built. SLS is like SLM conceptually, except that the material is being sintered in its solid state instead of being liquified as it is in SLM. Compared to SLM and SLS, EBM uses an electron beam as the heat source instead of a laser, and a vacuum chamber instead of inert gas [45]. An in-depth analysis of PBF is given in Gibson et al. [46].

Table 1
Brief history of metal additive manufacturing technologies.

Technology	ASTM Category	Invented	Ref.
Sequential Layer Deposition	DED	1982	[37]
Selective Laser Sintering	PBF	1989	[38]
Electron Beam Melting	PBF	1992	[39]
Selective Laser Melting	PBF	1995	[40]
Laser Metal Deposition	DED	1996	[41]
Electron Beam Additive Manufacturing	DED	2013	[42,43]

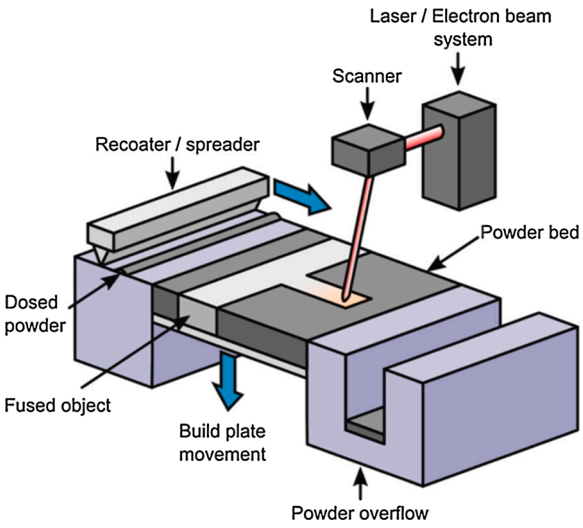

Fig. 1. Schematic of SLM PBF process [47].

2.2. Directed energy deposition

DED forgoes a powder bed and instead uses focused thermal energy to melt metal powders as they are being deposited [36]. Like PBF, DED can be used for polymers, ceramics, and metals, although ongoing research is primarily geared towards metal-based DED as reviewed in Dass and Moridi [48]. Raytheon Corporation first proposed wire- and powder-based sequential layer deposition (SLD) in 1982 [37]. Laser metal deposition (LMD), one of the first viable DED techniques, was developed by the Sandia National Lab in 1996 [41]. Electron beam additive manufacturing (EBAM), a technique reminiscent of EBM but for DED instead of PBF, was developed by Sciaky Incorporated in 2013 [42,43]. Analogous to PBF's foundational significance, LMD and EBAM are fundamental to various derivative DED techniques.

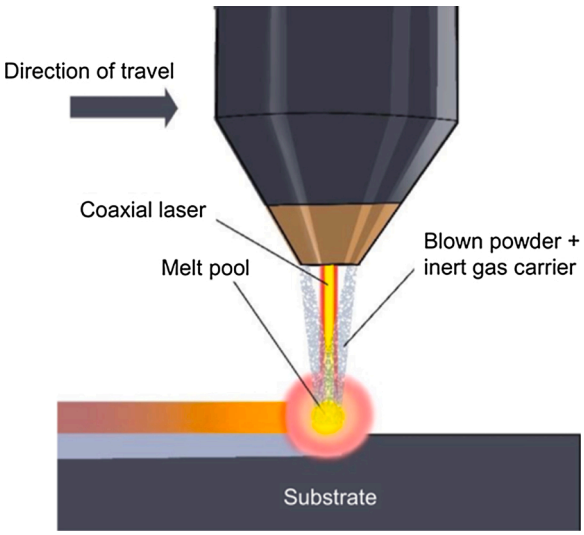

Fig. 2. Schematic of LMD DED process [52].

Fig. 2 shows a typical LMD setup. A laser is used to melt a small region of the substrate beneath the current layer, creating a melt pool. Simultaneously, a deposition system feeds metal powder or wire into the laser where it liquifies and joins with the melt pool before solidifying. The laser and deposition system travel together in three-dimensional space and build the part layer-by-layer until it is completed. Like PBF, LMD relies on toolpaths generated using CAD data. However, unlike PBF, DED does not need an enclosed build chamber since material is fed by an inert gas stream which prevents oxidation at the melt pool [49]. Additionally, since DED deposits material as it is needed and does not utilize a powder bed it is not constrained to deposition orthogonal to the build platform. Consequently, the deposition system can be dynamically tilted and rotated during the production process to achieve more desirable geometrical and mechanical properties [50]. A detailed description of DED process mechanics is provided in Gibson et al. [51].

2.3. Quality challenges in metal AM

Despite their advantages, both PBF and DED suffer from drawbacks unique to additive processes. Among these drawbacks, microstructural defects, porosity, dimensional accuracy, and surface roughness have attracted substantial research over the past decade.

2.3.1. Microstructural defects

Due to the additive nature of PBF and DED, the final part microstructure is highly dependent on deposition parameters. Most current literature focuses on metallurgical features such as melt pool morphology, precipitate behavior, dislocation density, grain size, and grain orientation for most of the typical alloys used in PBF and DED, such as aluminum alloys, stainless steels, tool steels, nickel-based superalloys, and titanium alloys [53]. Overall, AM microstructure exhibits highly nonconventional grain shapes, sizes, orientations, and gradients, as shown in Fig. 3. However, this nonconventionality is not considered defective as it would be in bulk material (cast, forged, rolled, etc.), but rather a characteristic of additive material deposition.

The unique characteristics of metal AM microstructure is shown in the following aspects:

(1) Cellular microstructure and columnar microstructure perpendicular and parallel to the build direction, respectively [6,54,55]. Furthermore, the microstructures exhibit strong texture due to the combined effect of epitaxy formation between the layers and temperature gradient along the build direction [56,57].
(2) Large fractions of random high-angle grain boundaries (HAGB, >10°) and low-angle grain boundaries (LAGB, 2°–10°) in the as-deposited materials, with a broad grain-size distribution and ripple-like grain shapes [6,54].
(3) High density of dislocations decorating the cellular walls with relatively clean grain interiors [54]. The size and the wall thickness of these solidification cells are known to be connected to the solidification conditions (e.g., thermal gradient, cooling rate, solidification front velocity) during the SLM process.

These deviations from "classical" morphologies are significant since they do not have the same extensive literature support as non-additive materials do. Many fundamental predictive relationships in material science, e.g., the Hall-Petch relationship between part grain diameter and yield stress [58], were empirically found decades ago based on observations of bulk materials and have been studied extensively ever since. However, relationships like this have not yet been definitively proven (or disproven) to exist in metal AM. Additionally, since the Hall-Petch relationship is empirical, it relies on material-specific and experimentally derived coefficients and exponents. Related data is abundant for bulk materials, but not yet for additive materials. Lastly, given that the complexity involved in AM-specific manufacturing processes can significantly complicate material qualification as compared to bulk materials, it may be difficult to establish "rule of thumb" relationships such as Hall-Petch for DED and PBF. Qualifying metal AM is location-dependent, and the homogeneity assumptions of "classical" methods are challenged and require systematic research to provide meaningful guidance for AM process analysis and characterization.

2.3.2. Porosity

A major drawback of metal AM-produced parts is porosity, which is detrimental to mechanical properties such as strength and fatigue behavior. Using SLM as an example, four predominant pore types can be found, as shown in Fig. 4 [59–61].

Adjusting process parameters such as laser density and scanning speed, as well as using post-process methods such as heat treatment, have been shown to reduce porosity. Fig. 5 shows computed tomography images of a Ti-6Al-4V sample made via SLM [62]. After hot isostatic pressing (HIP), no pores were found to be larger in diameter than the resolution limit of 22 μm, indicating a substantial reduction in porosity. However, despite their success, these postprocessing steps further complicate and disincentivize metal AM as a manufacturing process compared to traditional manufacturing processes. This indicates that pores should ideally be prevented altogether during the deposition

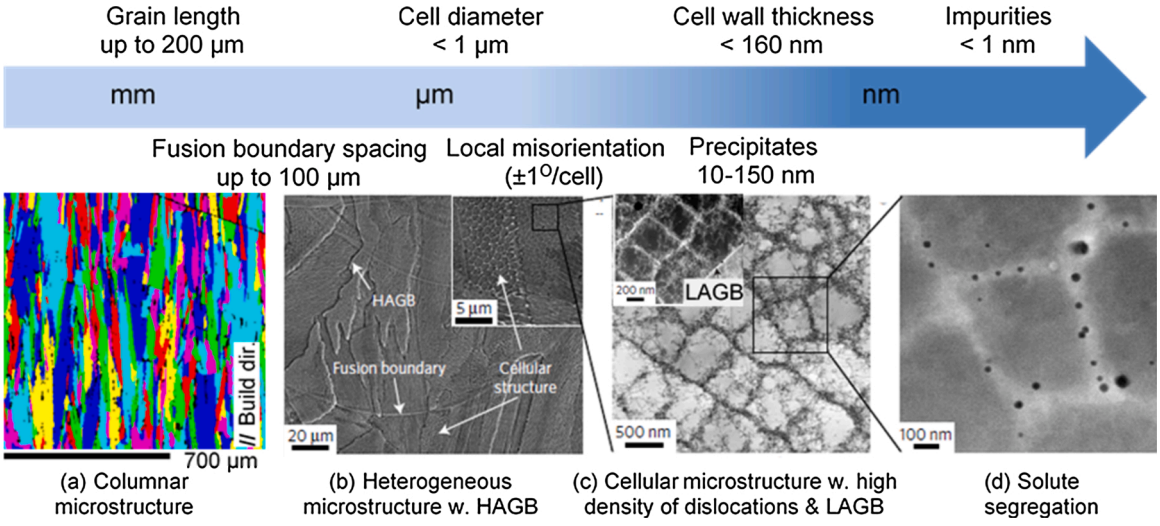

Fig. 3. Nonconventional microstructures found in SLM [6,54,55].

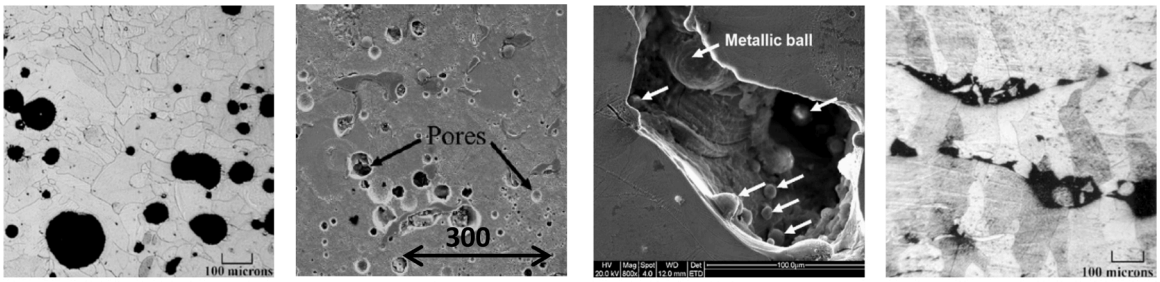

Fig. 4. Typical porosity of SLM part. (a) gas-induced pores [59]; (b) oxide-induced pores [60]; (c) balling-induced pores [61]; (d) lack-of-fusion-induced pores [59].

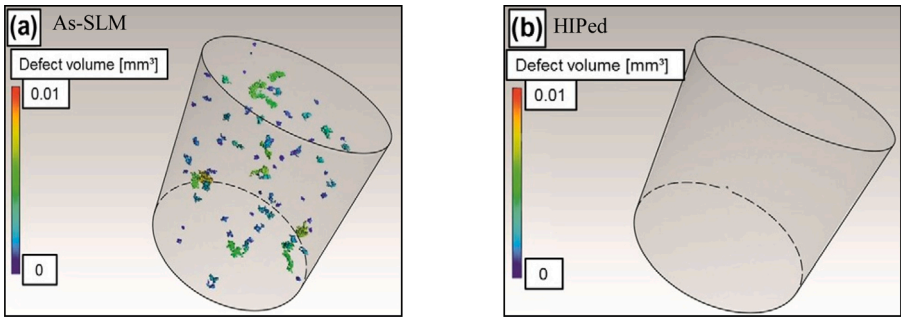

Fig. 5. Computed tomography images of Ti-6Al-4V specimens (a) before and (b) after hot isostatic pressing [62].

process.

2.3.3. Dimensional accuracy and surface roughness

Potentially substantial geometrical deviation (GD) and poor surface roughness (SR) of metal AM parts represent additional major drawbacks of metal AM processes. For example, neither PBF nor DED can currently compete with conventional machining's SR and GD, which are in the range of 1−10 μm [63] and 10−40 μm [64], respectively. SLM has an average SR of about 10 μm and an average GD of 40−80 μm [65–68]. For LMD, SR is on the order of 40 μm and GD is on the order of 20 μm perpendicular to the deposition direction and 400 μm parallel to the deposition direction [69,70]. Additionally, the SR of powder-based LMD parts is strongly dependent on the powder's particle size [41] and delivery rate [71], with smaller particles and lower delivery rates resulting in a smoother surface finish. Thus, controlling the surface finish of LMD components is much more challenging than doing so for conventional subtractive manufacturing techniques.

2.3.4. Residual stress and other challenges

Besides the challenges described above, additional quality issues exist for metal AM. For example, high residual stress is a commonly observed defect for AM-fabricated parts and often leads to cracking and warping failure modes [72]. Additionally, metal AM parts suffer from anisotropic mechanical behavior, which in general express themselves as lower tensile strength, and higher ductility when force is applied normal to the build direction as compared to when it is applied parallel to the build direction [73]. This is especially an issue for high load and long-cycle applications wherein an overly ductile structure may fail due to excessive loading or fatigue [74,75]. Metal AM anisotropy can be reduced via post-heat treatment.

Further challenges associated with metal AM processes include longer build times, complicated post-processing, and a more expensive workflow as compared to subtractive processes, both in terms of the equipment and material cost [76]. Last but not least, the limited material options for metal AM [74] and the difficulty in creating multi-material designs make it more difficult to make a case for metal AM technology [77]. However, recent advances in ML have demonstrated a promising pathway to mitigate the above issues and have offered the possibility of performance prognosis of metal AM parts, as discussed in the following section.

3. Machine learning for metal AM

As non-intrusive sensing methods have continued to improve, metal AM workflows have attained greater process repeatability. This is due to online process monitoring sensors that have increasingly shown their potentials to assist in formulating robust quality control measures and consequently, help build reliable and cost-effective metal AM parts. This is rightfully so, as ML models' ability to discover hidden patterns in high-dimensional and multi-modal data is well-suited for the multivariate and sensor-rich metal AM environment. ML for AM, from sensing pipelines to model outputs, is discussed in detail below.

3.1. Metal AM sensing

The primary enabler of ML-based methods is data ingestion, which has been aided by the continued advancement of in-process sensing technology. Information can be collected from the design, fabrication, and finishing stages of metal AM and used to train new ML models or feed pre-trained ML models for fast, automatic decision-making. Based on the specific sensor type and in-process stage of data collection, sensing data can be categorized into several categories. Each category has unique characteristics as shown in Table 2.

3.2. ML for AM prognosis

ML has shown to be an effective tool for metal AM quality prognosis, where prognosis is treated as either a classification or regression problem. Based on the relationship between *in-situ* data and AM properties, the prognostic analysis targets different quality issues, including those discussed in Section 2.3, as summarized in the following sections.

3.2.1. ML overview

ML models refer to computer algorithms that learn decision-making

Table 2
AM data sources and usage [78–97].

AM Stage	Data	Data Properties	Uses in ML	Ref.
Design	Process parameters	• Represent design information, process conditions • Rarely require preprocessing	• Find correlations between process parameters and part quality issues • Connect planning and fabrication • Parameter optimization and process control	[27, 78-81]
Fabrication	In-situ thermal images	• Capture full profile of part and spatiotemporal correlations • Usefulness ∝ sensor res.	• Develop models that learn spatial relationships, e.g., convolutional • Characterize spatiotemporal correlations • Real-time quality monitoring, closed-loop process control	[20, 82-90]
	Time series	• Reflect certain metrics of interest, e.g., pointwise temperature in melt pool • Less informative than images		[91, 92]
	Acoustic signals	• Reflect certain mechanical properties of fabricated part • Usually require time-frequency transform		[23, 24, 93]
Post-process inspection	Part quality metrics	• Scalar metrics for macro- or microstructural defects, e.g., properties, microstructures	• Find correlations between *in-situ* data, process parameters, part quality • Online or offline quality prognosis • Process parameter optimization	[20, 82, 85, 86, 94-97]

rules from data [98]. Generically, model f with trainable parameters $\boldsymbol{w} \in W$ operates on input instance $\boldsymbol{x}_i \in X$ and outputs prediction $\hat{\boldsymbol{y}}_i \in Y$, i.e., $f(\boldsymbol{w}, \boldsymbol{x}_i) = \hat{\boldsymbol{y}}_i$. Here, $\boldsymbol{w}$, $\boldsymbol{x}_i$, and $\hat{\boldsymbol{y}}_i$ are vectors within W, X, and Y, which are the multi-dimensional domains of parameters, inputs, and outputs, respectively. ML models are trained by finding the $\boldsymbol{w}$ such that the expected discrepancy, or "loss", between the prediction $\hat{\boldsymbol{y}}_i$ and the ground truth value $\hat{\boldsymbol{y}}_i \in Y$ is minimized across all i in the training dataset. This optimization procedure is specific to each model architecture, although gradient descent algorithms are widely used. Following training, ML model performance is quantified by measuring the loss with a validation dataset, which is disjoint from the training dataset. This measures the model's generalizability to novel data and thus quantifies its post-training quality.

ML training is conventionally categorized into supervised, semi-supervised, unsupervised, and reinforcement learning based on characteristics of the training data [99]. In supervised learning, f receives $\boldsymbol{x}_i$ and its corresponding $\boldsymbol{y}_i$ so that the loss can be calculated for every i in the training dataset and used to update $\boldsymbol{w}$. This optimization process is the "learning" part of ML. Supervised ML models include multilayer perceptrons (MLP), support vector machines (SVM), classification and regression trees (CART), and k-nearest neighbors (KNN), all of which depend on the value of the loss to learn.

Since the objective of supervised learning is to mitigate the discrepancy between predictions and the ground truth values, it is best-suited and widely used for predicting metal AM part characteristics, including mechanical properties, defect category, surface roughness, and microstructure. These approaches constitute most current literature in ML for metal AM, as shown in Sections 3.2.2 and 3.2.3, respectively. Also note that the decision logics of CARTs and SVMs are much more transparent and easier to interpret than MLPs and the KNN algorithm, for example, but also that the former models may be less accurate than the latter models [100]. Therefore, the practical needs for selecting a supervised learning architecture should be justified and determined first to determine if performance or interpretability takes precedence.

Unfortunately, labeling every training instance for supervised learning can require an inordinate number person-hours if done manually. Semi-supervised learning circumvents this problem by relaxing the 1:1 labelling requirement and allowing some $\boldsymbol{x}_i$ to be without ground truth $\boldsymbol{y}_i$. Instead, $\boldsymbol{y}_i$ for these unlabeled $\boldsymbol{x}_i$ are inferred by way of clustering or regression techniques. All $(\boldsymbol{x}_i, \boldsymbol{y}_i)$ pairs, including those with inferred labels, are then used to perform model training similarly to fully supervised learning [101].

While appealing conceptually, semi-supervised learning has few current applications in ML for metal AM because of two reasons: 1) data overabundance is not yet a problem in metal AM, and 2) metal AM label inference models are still in the early stage of development and must be thoroughly validated before they can be used to enable fully supervised learning of partially labeled data. However, continued investment in metal AM will gradually address the former problem and the latter problem is being actively addressed in literature, such as by the tensile property regression model by Xie et al. [102] and the process condition classification model by Li et al. [103]. For these reasons, the utility of semi-supervised learning in metal AM is expected to increase over time.

In contrast to supervised learning, unsupervised learning ignores labels entirely and instead seeks to find underlying patterns in the input data. The approach is widely used for clustering analysis using the k-means and hierarchical clustering algorithms. These algorithms are often used as components of other ML algorithms, such as the label inference system in a semi-supervised algorithm [104]. Unsupervised learning therefore has the same utility and limitations in metal AM as described in the above paragraph.

Reinforcement learning (RL), on the other hand, is disparate from the prior three types because it trains the algorithm, also known as an "agent," *via* a reward-and-penalty mechanism. RL is usually applied to sequential decision-making rather than parallel decision-making since RL agents operate using a Markov decision process wherein the agent's next action is determined by the current state of its environment. When an agent receives the state of its environment ($\boldsymbol{x}_i$), the agent acts on the environment to change it (according to $f(\boldsymbol{w}, \boldsymbol{x}_i) = \hat{\boldsymbol{y}}_i$) and then assesses if its action helped achieve its objective, e.g., maximizing AM yield stress. Beneficial actions are "rewarded" and detrimental actions are "punished," thus "reinforcing" good behavior [105]. Since it enables goal-seeking sequential decision making, RL is best suited for real-time metal AM process control wherein agent's actions are machine setting adjustments. This machine control paradigm has been recently realized by Ogoke and Farimani who used deep RL to decrease PBF melt pool depth control error by 91 %, which created more consistent mechanical properties throughout the produced parts [106]. RL can also be used in

classification and regression problems.

The following subsections will review existing studies in metal AM that leveraged ML for prognostics. The ML models used are introduced and the data types and prognostic problems concerned are provided. These materials present an overview of previous successes and illustrate when and how machine learning models have been used in metal AM. (Since this paper is focused on metrology as outlined in Section 2.3 rather than process control, RL-driven control systems are not discussed in this paper and we refer readers to the review in [107] instead.)

3.2.2. Classification tasks

A summary of previous research on classification tasks in metal AM is shown in Table 3. These tasks come in two predominant types: fault detection and category prediction.

Fault detection is a binary classification problem in metal AM that usually seeks to determine if a flaw is present or not. The success of a binary model is typically expressed in terms of the following metrics: *precision*, *recall*, F_1 score, and *accuracy*, as defined in Eqs. (1)–(4). While precision measures the fraction of detected flaws are truly flaws, thus reflecting upon the validity of the detection result, recall represents the fraction of flaws that are detected, indicating the completeness of the result. As a widely used metric, F_1 considers precision and recall with equal weight, and is useful for the scenarios when, for example, the model outputs the same prediction every time, which would mean a perfect recall but imperfect precision. Finally, accuracy is the ratio of correct predictions to the total number of predictions.

$$Pr = \frac{\text{true positives}}{\text{true positives} + \text{false positives}} \tag{1}$$

$$Re = \frac{\text{true positives}}{\text{true positives} + \text{false negatives}} \tag{2}$$

$$F_1 = 2 \bullet \frac{\text{Pr} \bullet \text{Re}}{\text{Pr} + \text{Re}} \tag{3}$$

$$Ac = \frac{\text{true positives} + \text{true negatives}}{\text{total number of predictions made}} \tag{4}$$

Category prediction is a multi-class problem that can take various forms. Fault categorization, e.g., pore type, surface defect type, is a common objective for these predictive models in metal AM. Since precision and recall are not well-defined for multi-class problems, accuracy is generally used to quantify model success.

3.2.3. Regression tasks

ML-driven regression models for metal AM in the literature are summarized in Table 4. In contrast to classification, regression tasks seek to estimate a variable of interest with as little error as possible. This is a common goal in metal AM when quantifying defect severity and predicting part properties such as yield stress and fatigue. Error quantification is done by comparing the difference between model predictions and ground truth values across a set of N predictions. This error can be quantified in direct terms, such as root mean squared error (RMSE) shown in Eq. (5) and mean absolute percentage error (MAPE) shown in

Table 3
Prior studies using classification for metal AM performance characterization [108–122].

Task	Process	ML	Model Input	Model Output	Metric	Ref.
MP	DED	SVM	Predicted temperature, in-situ sensor data	Incipient flaw present	F_1: 90%	[85]
		SVM	Spectrometer data, plume images	Lack of fusion severity category	F_1: 85%	[87]
	PBF	CART	X-ray image, acoustic emissions	Structural condition category	Ac: 95%	[108]
		CNN	Cross-sectional image	Defect category	Ac: 99%	[89]
		CNN	Cross-sectional image	Cracks present	Ac: 100%	[109]
		CNN	Plume images	Deposition morphology category	Ac: 93%	[110]
		CNN	Voxelated cross-sectional image	Anomaly present	F_1: 94%	[111]
		DBN	Deposition track images	Melt condition category	Ac: 83%	[112]
		MLP	Cross-sectional image	Incipient flaw present	Ac: 93%	[113]
		SVM	Cross-sectional image	Defect category	Ac: 80%	[114]
PP	DED	DT	Melt pool geometrical features	Pores present	Ac: 99%	[115]
		KNN	Melt pool thermal image	Pores present	Re: 98%	[20]
	PBF	CNN	Acoustic emission	Porosity severity category	Ac: 89%	[23]
		CNN	Powder bed image	Porosity severity category	F_1: 97%	[116]
		CNN	Powder bed image	Pores present	Ac: 97%	[117-119]
		KNN	Melt pool pyrometer data	Pores present	Ac: 94%	[91]
		MLP	Optical spectroscopy signal	Porosity severity category	F_1: 90%	[95]
		RL	Acoustic data	Porosity severity category	Ac: 82%	[24]
		SVM	Cross-sectional image	Pores present	Ac: 89%	[86]
GDP	DED	-	-	-	-	-
	PBF	CNN	Cross-sectional image	Defect present	Ac: 93%	[113]
SRP	DED	KNN	Laser scanner data	Surface defect category	Ac: 93%	[120]
	PBF	CNN	Cross-sectional image	Surface condition category	Ac: 99%	[121]
MPP	DED	-	-	-	-	-
	PBF	CNN	Melt pool images	Destructive test result category	Ac: 99%	[122]
		GMM	Features of photodiode data	UTS category	Re: 77%	[97]

Table 4
Prior studies using regression for metal AM [123–134].

Task	Process	ML	Model Input	Model Output	Metric	Ref.
MP	DED	-	-	-	-	-
	PBF	-	-	-	-	-
PP	DED	-	-	-	-	-
	PBF	MLP	Optical emission spectroscopy signal	Pore size	RMSE: 14%	[95]
		MLP	Spreader translation speed, rotation speed	% of layer that is pore	R^2: 0.99	[123]
		RF	Part position, orientation, powder composition	Pore diameter	r_p: -0.3	[124]
GDP	DED	MLP	Cross-section width, depth, height	Laser power, scan speed, powder feed rate	MAPE: 2.0-5.8%	[125]
	PBF	CNN	Layer image	Build quality metric	R^2: 0.8-0.98	[126]
		CNN	Thermal history, process parameters	Part distortion	RMSE: 24 μm	[127]
		SVM	Chemistry of powders, thermal properties, process parameters	Melt track width, depth, height, area below/above substrate	R^2: >0.9 (width, depth, area below), 0.75-0.85 (height, area above)	[128]
SRP	DED	GAANFIS	Laser scanner data	Surface roughness	R^2: 0.93	[129]
	PBF	GPR	Cross-sectional image	Surface roughness	R^2: >0.9	[130]
MPP	DED	CNN	Time-frequency images from thermal history	EL, UTS, YS	MAPE: 6.55%, 6.20%, 5.56%	[131]
		GPR	Alloy composition, heat treatment information	YS	R^2: 0.99	[132]
	PBF	GPR	Alloy composition, oxygen content, cooling rate	YS	R^2: 0.98	[132]
		MLP	Strut geometry data	SS, UTS, YM	MAPE: 9.39%, 5.26%, 14.60%	[133]
		NFI	Process parameters	Fatigue life	RMSE: 11-16%	[134]

Eq. (6), or in relative terms, such as coefficient of determination (R^2) as shown in Eq. (7) or Pearson correlation coefficient (r_p) as shown in Eq. (8).

$$\text{RMSE} = \sqrt{\frac{\sum_{i=1}^{N}(\hat{y}_i - y_i)^2}{N}} \tag{5}$$

$$\text{MAPE} = \frac{100\%}{N}\sum_{i=1}^{N}\frac{|\hat{y}_i - y_i|}{y_i} \tag{6}$$

$$R^2 = 1 - \frac{\sum_i(\hat{y}_i - y_i)^2}{\sum_i(\bar{y} - y_i)^2} \tag{7}$$

$$r_p = \frac{\text{Cov}(\hat{y}, y)}{SD(\hat{y}) \cdot SD(y)} \tag{8}$$

4. Towards physics-informed machine learning for metal AM

Previously reported work in ML for AM has improved metal AM quality control. A summary of the benefits ML in AM is shown in Fig. 6. However, current ML applications in AM still suffer from myriad problems inherent to ML in general, including an inordinate need for data and a lack of physical interpretability in the context of metal AM processes. For instance, while melt pool images are commonly used as inputs to ML models, those models do not develop a physics-based understanding of the complex thermomechanical phenomena taking

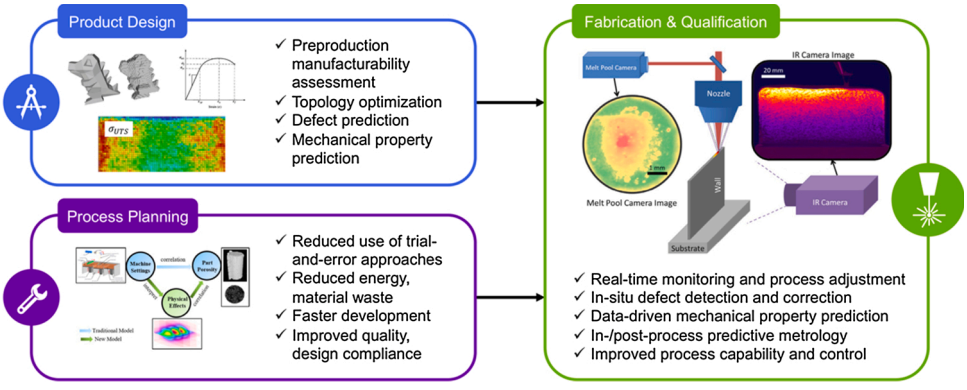

Fig. 6. Summary of ML benefits in AM; images from [131,135–137].

place and being observed by thermal imaging systems. This can lead to the models learning spurious relationships between image features and part properties since no domain-specific knowledge is utilized nor are any domain-specific constraints imposed, such as heat transfer laws. In short, current ML models excel at finding statistical correlations between inputs and outputs but may do so at the expense of the laws of nature: they are not constrained by physics. To remedy this ongoing issue, a paradigm shift from ML to physics-informed ML (PIML) for metal AM is proposed. This section presents background on PIML and discusses previous successes of PIML in metal AM.

4.1. PIML background

PIML is a branch of hybridized ML that incorporates the physics/domain knowledge of AM applications into ML model inputs, outputs, architecture, and training. A literature review has shown that there are five predominant ways to integrate physics into ML: 1) model input, 2) model training, 3) model components, 4) model architecture, and 5) model output.

In **physics-informed model input** (PIMI), *in-situ* production data is preprocessed to extract hidden physical information and/or augment it with production parameters and simulation data to better model the system being studied. An example of the former method is found in Xie et al. [102] wherein time-temperature series are projected into the time-frequency domain using wavelet transforms. This transformation extracts frequency information that is otherwise hidden in the time-domain signal and enables a deep convolutional neural network to consider frequency and time information simultaneously and predict tensile properties using this information. This approach has the potential to be used for deductive reasoning, i.e., using pre-established physical principles to select input features that are likely good predictors of the output variable(s), as well as inductive reasoning, i.e., crafting novel features, assessing their predictive power with respect to model output (s), and determining *post hoc* why the features are good or bad predictors in terms of physics.

Another pillar of PIML is **physics-informed model training** (PIMT). The goal of this technique is to ensure physical consistency between model inputs and outputs by penalizing output spuriousness *via* the loss function [141]. This is seen in the lake temperature modelling MLP designed in Karpatne et al. [138]. In this work, the physical behavior of interest is the monotonic increase in lake water density as a function of depth below the surface, i.e., $\rho(d)$. The physical model expects that as d increases, ρ will increase as well. Therefore, if the MLP predicts that ρ has decreased between two successively deeper d, i.e., $\rho(d_1) > \rho(d_2)$ for $d_1 < d_2$, then the loss function for the current iteration is increased by $\lambda(\rho(d_1) - \rho(d_2))$ where λ is a scaling constant. If the density change is physically consistent, i.e., $\rho(d_1) \leq \rho(d_2)$, then no penalty is applied. Since the MLP training process seeks to minimize the loss function, it maximizes physical consistency by attempting to achieve $\rho(d_1) - \rho(d_2) \leq 0$ for $\forall\ d_1 < d_2$.

Just as loss functions can be physics-informed, so too can model mechanisms such as activation functions and initialization procedures. This kind of mechanistic alteration is the central idea of **physics-informed model components** (PIMC). Activation functions are good candidates for infusion with physical intuition since usual activations, e.g., sigmoid, hyperbolic tangent, and rectified linear unit, are usually selected only because they work well and not because they carry physical meaning.

Howland and Dabiri [139] recognized the shortcoming of physically meaningless activation functions when modelling wind farm power output and subsequently modified an activation to be physically meaningful. A directed acyclic graph was developed to model power generation relationships between turbines on a farm considering the fluidic wakes between them. The power generation of a turbine in layer i (P_i) was modeled as a weighed sum of the turbines in preceding layer j, i.e., $P_i = \Sigma_i\ w_{i,j}P_j$. To capture the nonlinear fluidic wake interactions between successive layers of turbines, the sigmoid function was modified formulaically to fit a thrust coefficient curve as a function of P_j, i.e., $C_T = \sigma_{CT}(P_j) = (2.03)^{-1}[(1 - e^{-2(P_j - 2)} + \varepsilon)^{-1} + 2.03]$ where $\varepsilon = 10^{-8}$ for numerical stability. This alteration scaled, translated, and reflected the traditional sigmoid curve $\sigma(x) = (1 + e^{-x})^{-1}$ while keeping σ_{CT} bounded within (0,1) like the traditional sigmoid. The modified activation was physically meaningful since it was designed to predict downstream power (W) as a function of upstream power (W), rather than "activation units" as a function of "activation units" as is the case with non-PIML activation functions. The power generation model was then expressed as $P_i = \Sigma_i\ k_{i,j}P_j\ \sigma_{CT}(P_j) + c_{i,j}P_j\ [1 - \sigma(P_j)]$ where k and c are learnable matrices which dictate the model behavior at low and high values of P_j, respectively. A genetic algorithm was then used to find the optimal k and c that minimized the model's loss.

Physics-informed model architecture (PIMA) is another promising pathway to achieving PIML. In this technique, the way in which an ML model represents input information is trained during model optimization to conduct physically meaningful analysis. This differs from PIMC since architectural changes fundamentally alter the data representation whereas the model components change how the data is processed without changing the data itself. PIMA also differs from PIMI in the sense that PIMI's input data transformations are static whereas PIMA's transformations are learned as part of the ML model. PIMA-driven transformations are only possible if the transformation is trainable, which often equates to being smoothly differentiable in the case of gradient descent-based algorithms. Finding differentiable formulations of input transformations may not be a simple process, so PIML developers must decide if learned PIMA transformations are worth the time and energy spent formulating them as opposed to using quicker but manual PIMI.

A recent example of PIMA is the CNN-based WaveletKernelNet by Li et al. [140], which automatically extracts frequency information from an incoming one-dimensional time series. It does so by replacing the first layer's convolution kernels with n trainable wavelets, each with scale and translation parameters s and u, respectively. The first layer thus outputs n one-dimensional convolutions of the original time series, which are further processed by the remaining one-dimensional convolutional layers to arrive at a model prediction. By implementing backpropagation-based model optimization, the s and u parameters of the n wavelet kernels in the first layer are optimized to reduce the model's loss. Since the form of the wavelet can be controlled, e.g., Morlet or Mexican hat, the user is able to choose the wavelet formulation that best captures the physics hidden in the input time series. Methods for doing so are demonstrated in Yan and Gao [141].

Finally, **physics-informed model output** (PIMO) refers to the idea of assessing a model's prediction logic for physical consistency. This differs from PIMT in the sense that PIMT's loss functions measure model performance against ground truth values or physical phenomena whereas PIMO's prediction logic examination explains how a model arrived at its prediction. Techniques such as layer-wise relevance propagation (LRP) [142]. Linear Interpretable Model-agnostic Explanations (LIME) [143], and Shapley additive explanations (SHAP) values [144] can be used to achieve this logical analysis. Each of these techniques reveal not only what input features are relevant to ML model prediction logic, but also how those inputs numerically affect the model output.

For instance, LRP was implemented by Grezmak et al. when performing motor fault diagnosis as shown in Fig. 7 [145]. Vibration signals measured on an induction motor were first processed by wavelet transform to generate time-frequency images, which were subsequently classified into one of four fault types using a two-dimensional CNN. Following network optimization to 100 % classification accuracy, LRP was used to visualize which parts of the images contained the most useful information when performing classification. This effectively showed what areas of the image the CNN was "looking at" to perform classification and allowed for physics-informed assessment of what the

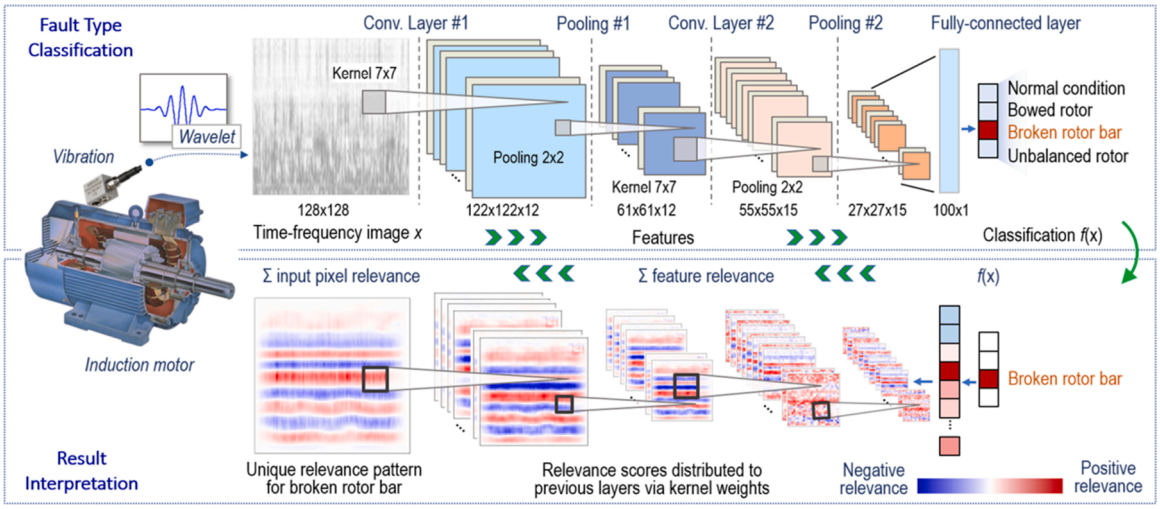

Fig. 7. Summary of LRP-based method by Grezmak et al. for achieving physics-informed model output [145].

CNN had learned and determination of if this learned knowledge was consistent with physics and previous literature.

4.2. PIML development

The prevailing advantage of PIML is that it enhances model interpretability and reduces model spuriousness by being rooted in physical principles. It does this while retaining the competitive performance ceiling of ML as well. Outside of manufacturing, PIML has been used to: 1) predict lake temperatures with less than 1 °C RMSE and complete consistency with physics [138], 2) solve the Schrodinger and Allen-Cahn equations with 0.002 and 0.007 L_2 error, respectively [146], 3) solve the Burgers equation with 3 % error in the coefficients [147], 4) solve elliptic stochastic partial differential equations to within 0.005 L_2 error [148], 5) simulate fluids up to 700× faster than classical simulation techniques [149], and 6) detect and track objects with 95 % correlation between predicted and actual position [150].

Within the manufacturing domain, PIML has been developed to: 1) predict specific cutting energy of milling with the accuracy of 1 J/mm^3 RMSE by integrating machine learning and process mechanics [151], 2) predict Taylor tool life equation coefficients with 5 % MAE [152], 3) predict milling tool wear with 6 μm MAE [153], 4) predict chatter with 99 % accuracy [154], 5) predict polymer AM ultimate tensile stress with 0.6 MPa RMSE [155], 6) predict DED yield stress with 9.2 MPa RMSE [156], and 7) predict DED pore diameter with 0.02 mm MAE [157], to name a few representative applications.

Another advantage of PIML is its synergistic integration of physical models and data-driven methods. The former is oftentimes reliant on simplifying or homogenizing assumptions to be tractable whereas the latter may deviate from the laws of physics, as previously discussed. Additionally, physical models of complex thermomechanical systems such as PBF and DED are infeasible to update in real-time due to the complexity of numerical simulation required to do so. Well-trained PIML models take advantage of physical and data-driven models (Fig. 8) as they are based on the laws of physics and respond to real-time data streams using the comparative computational efficiency of ML-based computation. Underlying fundamental ML architectures such as MLP and CNN also enable uncertainty quantification and prediction in PIML, as is done in physical experiments and statistical analysis. Techniques for doing so are reviewed in Kabir et al. [158].

4.3. PIML for metal AM

Though not yet widely adopted, PIML has achieved success in metal AM where several studies have explored the potentials of PIML for

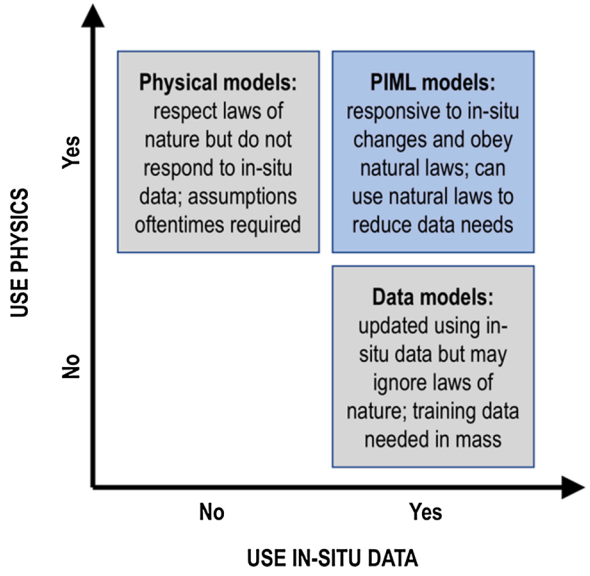

Fig. 8. PIML *vs.* physical and data-driven models, adapted from [154].

quality prediction. For example, PyroNet+ and PyroNet++ (Fig. 9) were proposed in a PIMI study by Guo et al. [157]. These PIML-driven NNs extracted features from thermal images of melt pools with a CNN and concatenated the features with physical measures from FEA simulations before feeding them to a subsequent MLP for porosity prediction. This is an example of supplementing *in-situ* data with simulation data to achieve PIMI. The features from thermal images encoded physically meaningful process parameters in the real-world, such as heat transfer, mass flow, and melt pool volume even though these features were not explicitly extracted from the *in-situ* data. The FEA features, such as melt pool length, provided guidance about what the CNN should have been seeing under ideal conditions. The juxtaposition between real-world physics and simulated physics gave PyroNet++ additional physically meaningful insight about the process. It could observe what the pyrometer should have been seeing and then infer porosity condition based on deviation from that idealized state. This contrasts with non-PIML methods which would have received the pyrometer data in isolation and found statistical (not physical) relationships between the images and the porosity. The external information, in the form of FEA, is the PIML-enabling mechanism of this study. PyroNet++ successfully detected pores *in-situ* with 100 % accuracy and predicted the diameter of

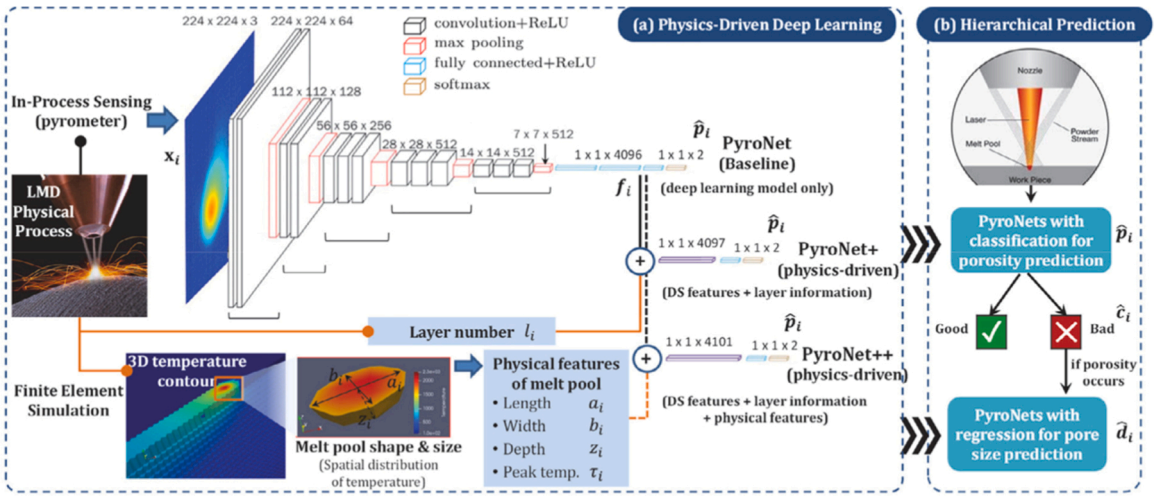

Fig. 9. PIML-driven PyroNet + and PyroNet++ in Guo et al. [157].

the pores with 0.03 mm MAE.

Similarly, Ren et al. [159] used achieved PIMI by gathering simulation data to develop a recurrent MLP to identify the correlation between laser scanning patterns and thermal history distributions. FEA was used to simulate a DED process and, crucially, keep track of when each voxel of material was deposited. This temporal information was critical in making the study PIMI-driven since it gives information that cannot be extracted from *in-situ* temperature data alone. This time-since-deposition matrix was used as the input to the developed model, which can predict the thermal field for an arbitrary geometry with different scanning strategies with 2 % MAPE compared to a ground-truth FEA simulation.

Liu et al. [136] minimized porosity and optimized machine settings using domain knowledge-based PIMI, which is distinct from simulation supplementation. Physical information related to energy density and pressure on the part were calculated using domain knowledge and became SVM inputs and the model regressed mean pore size to within 8 % MAPE. The advantage of using PIMI-crafted features for the SVM rather than *in-situ* observational values only was that "hidden" information such as photon momentum and radiation pressure could be used explicitly as inputs. Since these quantities are calculated with trigonometric functions and many ML techniques can only perform polynomial approximations, this hidden information would likely not be accurately extracted during the ML training phase and would need to be included via practitioners' domain knowledge. Additionally, since these physical mechanisms directly determine the process outcome, the developed method aimed to find *causal* relationships between inputs and outputs, which are much more useful that *correlational* relationships that are commonly found in standard ML.

Akin to Liu's domain knowledge inclusions, Nagarajan et al. [160] combined dimensional analysis conceptual modeling and classic ANNs to create a novel knowledge based MLP to achieve PIMA. A topology was defined for the topological zones derived from physical knowledge of the metal AM process and MLP-modeled zoning knowledge, which captured the system behavior and improved the repeatability of metal AM production. The developed model predicted AM product dimensions with 58 % less error than a conventional ML model.

In contrast to PIMI, which relies on simulations as model inputs, PIMT has been used to replicate metal AM simulations with a lower computational burden. Zhu et al. [161] embraced PIMT to introduce a physics-informed neural network (PINN) [146] for predicting thermal history and melt pool fluid dynamics in PBF. Real data from the process were processed by an MLP with a loss function constrained by physical laws to predict thermal history, fluid pressure, and fluid velocity. Unlike PIMI, this work used FEA simulations to inform the physics-constrained loss function and penalize the network when any of the three outputs deviated from the simulated ground truth. Additionally, partial differential equations modelling momentum, mass, and energy conservation along with their Dirichlet and Neumann boundary constraints were directly inserted into the loss function. This reduced the need for training data and expedited the training process by forcing the MLP to respect boundary conditions while also modelling the interior of the temperature-pressure-velocity output space. Had this physics-informed domain knowledge not been included in the loss function, the model would have relied on naïve, physics-uninformed gradient descent which would have been slower and ignorant of the boundary conditions, resulting in worsened interpolation and extrapolation. The model predicted PBF melt pool dimensions and cooling rate with as little as 2.9 % and 7.8 % MAPE, respectively, as compared to experimental measurements. These results were as good or better than FEA-derived predictions, and at a fraction of the computational cost.

There is notably little literature regarding PIMC, PIMA, and PIMO in metal AM. The absence of PIMC and PIMA are attributable to the growing yet young development horizon of ML for metal AM. Regarding PIMC, it is still not well understood how to make model components "look like" thermomechanical relationships found in AM (due to the complexity of these relationships) such as in Howland and Dabiri [139]. Using tried and true model components work well for the time being, but physics-integration is expected to come as a deeper understanding of metal AM physics is developed. As for PIMA, it is relatively unknown which information extraction techniques are best for metal AM right now. Xie et al. [131] demonstrated the utility of wavelet transforms in predicting DED tensile properties, which may be a path to PIMA, but widespread use of optimizable information extraction in metal AM is yet to be seen (though this does not detract from the merits of PIMA). PIMO's relative absence can also be traced to a still-developing understanding of AM physics. Without ground truth knowledge about metal AM physics, interpreting results in the spirit of PIMO is difficult and possibly even futile. However, there is a growing body of research on process-property relationships, such as between porosity and temperature distribution [162] and between cooling rate and tensile properties [135]. This body of observed relationships improve the utility of PIMO and make it a more promising technique in metal AM moving forward.

To summarize, PIML methods present a promising and powerful alternative to pure physics-based modeling and simulation or conventional ML-based process modeling and monitoring for metal AM. Previously reported success has demonstrated their potentials and shed light on multiple future research directions. Through the five-dimensional lens of PIMI, PIMT, PIMC, PIMA, and PIMO, existing literature has been categorized to assess current directions and progress

in achieving comprehensive PIML implementation. Still, challenges and practical concerns exist for PIML development, which are elaborated in the next section.

5. Challenges and outlook of physics-informed ML for metal AM

In AM and related fields, the transition from conventional ML to PIML is an ongoing process. The existing cases of PIML in metal AM (Section 4.3) have paved the way for its development. Yet, open issues have yet be solved. This section introduces a framework for implementing PIML methods in metal AM applications and discusses the challenges and potential opportunities. Data-related issues, practical concerns, and physical considerations are considered.

5.1. PIML implementation framework

Fig. 10 shows a proposed methodology for implementing PIML in manufacturing operations. The sequencing of the methodology is inspired by the life cycle assessment framework described within ISO 14040 [163]. Note that this workflow is like that of conventional ML with two distinctions: 1) initial assessment of PIML necessity, goals, and scope, and 2) mid-development verification of physical assumptions being included in PIML models. These two crucial steps ensure that the time to be spent developing PIML techniques and strategies will be meaningful, and that the final product is justifiable given the plethora of off-the-shelf black box ML models available that would exchange interpretability for reduced development time.

5.2. PIML challenges

PIML faces challenges primarily in the area of method development. These are discussed below from the perspectives of PIML data integrity, practicality, limitations, and cybersecurity.

5.2.1. Data availability

Data availability in AM is a key issue to the development of PIML. Due to its flexibility and high level of possible customization, metal AM applications tend to have low-volume production. Some commercial AM systems do not have built-in data acquisition systems and require sensors to be retrofitted, which increases operational costs [146,164]. Such a situation further leads to limited data availability in many AM applications. Several institutions have created benchmark datasets for metal AM [83], which have significantly boosted the utilization and development of ML and PIML approaches. Yet, these datasets represent metal AM in lab environments, instead of industrial metal AM applications. An industry-level data-sharing policy is imperative to further leverage PIML in metal AM [165] though this has yet to be developed and universally adopted.

Alternatively, process simulations can be developed to provide additional physically meaningful data to support the implementation of PIMI. Conveniently, this approach also enables high-efficiency RL agent training. Since RL is Markovian, it is well-suited for simulation-like applications where the process status at each time step is a function of immediately preceding time steps. Assuming a physically consistent AM process simulation environment is constructed (e.g., in the form of a digital twin), an RL agent can control the simulation parameters (laser power, scan speed, toolpath, etc.) and learn how to guide the AM process to achieve part property outcomes that are desirable to the user. Since this process is entirely virtual, the agent can be trained with theoretically infinite training scenarios. Furthermore, if the ML-based simulation produces sufficiently accurate process outcomes (part mechanical properties, surface roughness, etc.), it can also be used to train

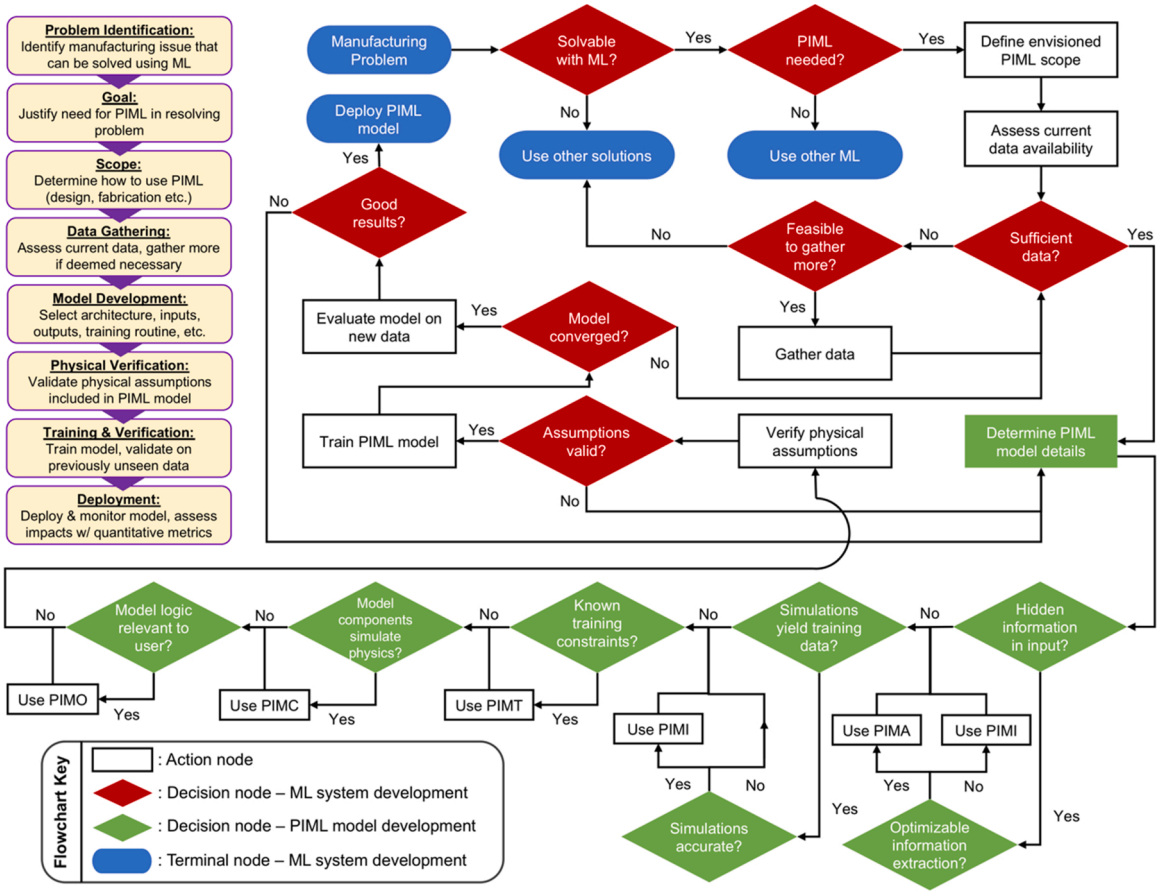

Fig. 10. Flowchart for PIML implementation.

supervised ML models for AM metrology. The benefit of this approach is that ML models often perform inference that is orders of magnitude faster than FEA simulations. However, such models require well-designed simulations to be established first to train the RL agents, which is another outstanding issue as discussed in Section 5.2.2.

5.2.2. Physical modeling limitations

Since they are often used as sources of PIML training data, metal AM physical models should be as accurate as possible. It is therefore important to recognize that physical modeling methods have inherent assumptions, simplifications, and approximations that detract from their accuracy [166]. While the past decade has seen significant progress in the development of novel modeling techniques, most of the existing physical models manifest limited coherence with data from actual manufacturing processes due to underlying assumptions. These span from domain-related limitations or machine process characteristics (e.g., laser diameter, hatch spacing) and laser/material interaction characteristics (e.g., absorptivity, optical penetration into the powder/bulk material), to material properties, (e.g., thermal conductivity, heat capacity, coefficient of thermal expansion, density, phase transition temperature) [166]. Furthermore, multi-scale (in terms of both space and time) integration over associated temperature ranges also introduces variability when predicting metal AM process characteristics.

Significant potentials exist in improving physics-based modeling and simulation of metal AM processes in terms of more accurately and robustly handling energy beam-material interactions, melt pool solidification, microstructure evolution, nonlinear temperature-dependent material properties, thermal history, process variations, and uncertainties [7]. By incorporating design formulations and parameters related to metal AM fundamentals into physical models, model variability can be minimized and new avenues to achieving PIML, such as the RL described in Section 5.2.1, can be opened [167,168]. Modeling methodologies pertaining to heat sources, material properties, microstructures, and state changes/phase transformations represent major research directions to predict and optimize the outcome of metal AM process prognosis via PIML.

5.2.3. Data imbalance

Data imbalance is another key issue impeding PIML. In many AM applications, the data related to noncompliant parts is miniscule compared to the compliant data. On one hand, limited data availability has constrained metal AM dataset sizes; on the other hand, the measurement of noncompliance-inducing defects, such as porosity, requires expensive tools, e.g., computed tomography [20] for analysis of part microstructure. This situation has led to an imbalance of data classes (compliant *vs*. noncompliant) for developing PIML, which impedes the characterization of the noncompliant parts using ML models. One way of alleviating data imbalance is resampling. Methods such as bootstrapping [169], image synthesis [170,171], and synthetic minority oversampling [172] have been demonstrated to reduce the detrimental effects of class imbalances on training ML systems. Additionally, techniques developed specifically to characterize minority classes, such as few-shot learning [173], Siamese/triplet networks [174,175], and isolation forest [176], can be used to study noncompliant specimens.

Another promising solution to imbalanced data is *granular computing*. This technique processes complex information entities known as "information granules" that are any subsets, classes, objects, clusters, and elements of a universe that are drawn together by distinguishability, similarity, or functionality [177]. As an example, granular computing can be applied to *in-situ* thermal images from AM to extract semantically meaningful geometric patterns. Analyzing the information granules from compliant and noncompliant data instead of the data themselves may alleviate the impact of dataset size. Meanwhile, granular computing may be incorporated in PIML model design to facilitate feature extraction from imaging or time series data, such as for semi-supervised learning, thus reducing the negative effect of data imbalance to model training.

5.2.4. Data curation

Data curation is another challenge. "Curation" here refers to the preparation of data for further analysis, such as cleaning, processing, alignment, and fusion [178]. In metal AM, the way of handling datasets should be guided by practical considerations. Based on where and what datasets are collected, the problems to be solved by learning from the data are predetermined. For example, with the justified connection between abnormal thermal dynamics in melt pool and porosity in DED metal parts [179], *in-situ* images of melt pool can be used to predict porosity [20,90,157]. Thermal images collected with two online sensors installed along different angles may show complementary profiles of a part being built during the AM process, and integrating these two data sources may improve the accuracy in prognostic analysis [180]. In that sense, understanding the underlying physics, mechanics, and materials in metal AM is as important as studying data from real-world production. Thus, interdisciplinary collaboration is required to guide data handling in PIML.

As a data-driven paradigm, PIML requires sufficient data for model training and validation. Data availability and curation are both critical. Without manually augmenting real-world data with simulation or resampling, small datasets are insufficient to develop robust PIML methods. When data are available but come with complex characteristics, data curation becomes the primary concern and must be done properly to ensure the validity of PIML methods.

5.2.5. Standardization of PIML methods

Due to its current novelty, standardizing PIML development has proven challenging. Not only do practitioners need to be well-versed in ML methods, but they must also have a thorough understanding of the physical mechanisms being modeled to effectively model these mechanisms using PIML. Our implementation framework from Fig. 10 indicates two candidate areas for standardization: determination of 1) whether an ML-based study should be considered to be PIML (2nd red decision node), and 2) which branch of PIML is suitable for a given problem (green decision nodes).

First, ambiguity may arise when determining if an ML study is physics-informed, especially to practitioners without domain knowledge. A likely scenario is that conventional ML approaches are falsely considered PIML, which dilutes the usefulness of PIML. For example, PIMI, as defined in Section 4.1, refers to the use of physics to *correct, enrich, or enhance* data collected from metal AM applications. It is therefore important to use domain knowledge about the physics of the application being studied to execute data transformation or processing to make this data physics-informed. The direct use of physical measures such as temperature or geometric deviation as inputs to conventional ML models, however, does not meet the PIMI definition but may still be mistakenly considered a PIMI approach. While it is tempting to call any ML model with physically meaningful inputs or outputs "physics informed," this temptation must be rejected since such models are not constrained and informed by the laws of physics. It is expected that more correct PIML/non-PIML characterization will occur as more individuals become aware of the definitions of PIML and its subcategories we provide in Section 4.

Second, since there are currently five branches of PIML methods, as defined in Section 4.1, selecting the suitable branches of PIML for an application can be difficult. It requires the practitioner to evaluate the available data and physical resources and have a clear idea of the consequences of integrating the physical resources with ML models at each stage (i.e., input, training, component, architecture, output). The practitioner must also identify what their desired outcomes are, what knowledge they seek to gain, and if the developmental overhead of PIML is worth the increased time costs compared to brute force and unexplainable conventional ML. These meta-level requirements are rarely fulfilled prior to initiating an ML-driven study. A systematic approach,

such as that presented in Fig. 10, is needed to breakdown the *a priori* PIML development considerations into more manageable and serialized phases, with clearly defined loops when PIML model development is unsuccessful. Like the ISO 14040 framework upon which it is based, the methodology in Fig. 10 makes the goal development and planning phase a prerequisite to the results acquisition, deployment, and reflection phase.

5.2.6. Horizon of model development

Another practical issue is the horizon of PIML, where "horizon" here refers to the stage and manner of how PIML can be used to aid in practical metal AM applications. As a hybrid of physics and data, PIML methods typically need more than one information source. Currently, PIML methods are mainly developed for applications that offer rich physical information and data simultaneously. This means the current PIML methods are mostly driven by feasibility in method development rather than practical needs. Consequently, brute-force use of PIML models in metal AM applications may create a gap between data-driven solutions and practical needs, limiting the contributions of PIML output to problem-solving. Restricted by limited physical understanding and data availability in metal AM, designing practically useful and feasible PIML methods remains a challenge.

5.2.7. Adversarial attacks

Another issue inherent to PIML and ML in general is adversarial attacks. Adversarial attacks are a broad family of methods meant to deceive ML algorithms and force them to output intentionally incorrect predictions. This deception is usually done very subtly so that humans cannot even recognize that anything has happened to a model. Attacks can be done to harm model training (sabotage), degrading post-training performance (fraud), and reverse-engineering the model (espionage) [181]. Methods for performing these attacks are reviewed in Mello [181] and Brendel et al. [182]. A previously verified and well-trusted model being subtly corrupted by malicious actors can have profound consequences in manufacturing, including theft of intellectual property, unpredictable part quality, and even death. Adversarial attacks are therefore one of the most consequential weaknesses of ML, especially in the context of AM for highly critical parts.

The threat of adversarial attacks has remained high on the list of alerts for cybersecurity experts and manufacturing practitioners. There is a vast body of literature on the topic of "hardening" ML models to make them less susceptible to adversarial threats. For example, Madry et al. [183] developed a robust neural network optimization method to ward off fraud attacks on classification models and charted a path towards ML models with *guaranteed* robustness. The method increased model accuracy from 6.4 % to 89.3 % when using poisoned evaluation data (MNIST digits) [184]. Anthi et al. [185] proposed a hardening strategy specifically for ML-controlled industrial control systems and considered the expanse of threats posed by an insider attack by a person with privileged access to physical control systems. The approached used adversarial training to reduce the attack success rate by 11 %.

Despite prior successful cases, adversarial attacking is a quickly evolving field with monotonically increasing cybersecurity research demands [186]. PIML developers must be aware of the inherent weaknesses in ML that can be attacked to mitigate manufacturing operation risk. Additionally, practitioners must be aware that current ML cybersecurity research is oriented towards conventional, non-physics-informed ML and that there is currently a negligible body of research on hardening PIML in particular.

5.3. PIML use case considerations and limitations

When using PIML in metal AM applications, there are several aspects to consider. Many of them are also found in conventional ML, although PIML does introduce some unique caveats and advantages. Major concerns stem from computational capability, data quality, and data variety, which are elaborated below.

5.3.1. Computing power

Although faster than physics-based methods like FEA, ML can still be computationally expensive. In practice, considerations arise for computational complexity and compute time. Metal AM systems may involve complex mechanics, physics, and material science. The layer-by-layer addition of materials in metal AM has enabled complex internal features, e.g., channels and embedding of prefabricated components, leading to residual stresses and dimensional warping that cause structural failures of the parts under normal operating conditions or even premature failures [187]. These physical systems are mainly characterized by PDEs, SDEs, or optimization models that are difficult to solve analytically [188]. PIML can incorporate such complex physics and provide a data-driven solution, e.g., PINN [146]. However, such PIML methods can be computationally complex and pose a high burden on computational resources. As such, implementing ML in large-scale production may come with a prohibitively high cost. A possible mitigation strategy is to increase PIML model coarseness (e.g., pixel/voxel size) and reduce the complexity of physics to be incorporated. Nonetheless, the computing resources necessary to train and implement a sufficiently accurate, robust, and trustworthy PIML model must be considered.

5.3.2. Data modality

The input data modality to a PIML system, e.g., images, time series, acoustic signals, is a major factor for model selection and data preprocessing. In the context of metal AM, ML is needed to perform decision making using a variety of input modalities, as shown in Section 3.1. Model selection must therefore consider the physical information available in the modality of interest. Two-dimensional CNNs are suitable for AM image processing due to their ability to detect geometric features such as cracks and pores, which affect the material's tensile properties. Recurrent NNs such as Long Short-Term Memory networks and related variants are promising if time series data, e.g., temperature signals, are being analyzed. This is because recurrent architectures are Markovian and are thus able to account for previous time steps' effect when making future predictions, such as the temporal evolution of a temperature field [105]. Alternatively, the underlying physics of an AM process may be extracted from the data. For instance, *in-situ* thermal images of DED and PBF melt pools have spatiotemporal correlations, which are not captured by standard CNNs [22]. In this case, a recurrent CNN would be necessary to capture the time-dimension correlation.

5.3.3. Data integrity

Another consideration is data imperfection [189,190]. Regardless of data modality, any ML model can be sabotaged by poor-quality training data under the colloquial "garbage in, garbage out" paradigm [191]. Data collected from factory floors are often noisy, redundant, or incomplete, and therefore of low quality, offering limited useful information from which to learn. Additionally, noisy training targets (y_i) can result in an ML model learning to predict the noise in addition to the true value. If the noise distribution changes between training and validation, the model's loss on the validation data is expected to increase substantially compared to the training data.

ML models are expected to be more robust and stable as a result of data pollution mitigation [192]. However, erroneous or misleading prior information being included within PIML models will pollute them from within and induce spuriousness. For this reason, assumptions made when developing PIML models need to be verified either experimentally or by using previous used and trusted data. While not every corner case can be enumerated, the physical and systems-level assumptions upon which PIML models rest must be rigorously established.

It is possible, though, for PIML to bypass data quality problems. Prior domain knowledge and expert opinions, e.g., deposition physics and equipment degradation paths, can act as supplementary information and be leveraged to mitigate the imperfection of real-world data using any of

the five PIML tenants in Section 4.1. Notably, prior information can be coded into ML models, such as physics-informed training algorithms and physics-informed activation functions, to strengthen the relevant information embedded in-field data and expedite model convergence [146].

5.3.4. Production volume and variety

Another consideration is production volume and variety. Due to its unavoidable need for training data, PIML (and ML in general) is best suited for producers of high-quantity, low-variety (HQLV) products. The reasons for this are three-fold: 1) low-quantity, high-variety (LQHV) production would require a variety-proportionate number of trained and verified PIML models based on different product geometry, material, and other characteristics, 2) LQHV production generates little data each production run, which makes timely PIML model development difficult, and 3) the time spent developing and verifying PIML models (or creating PIML training simulations) for LQHV production would likely exceed the amount of time necessary to conduct trial-and-error parameter tuning based on expert intuition and finish the production run without any PIML assistance [193]. Future work in PIML is recommended to focus on the generalizability of models across geometries, materials, machines, and process parameters to close the PIML utility gap between LQHV and HQLV production.

6. Conclusion

This paper provides a comprehensive summary of prevailing metal AM techniques and outstanding issues in quality control while showcasing successes of ML in addressing quality issues. It also proposes a paradigm shift from pure data-driven ML to PIML. The fundamental concepts and rationale of PIML are established and previous PIML cases, along with key PIML implementation considerations, are investigated. As an emerging topic, PIML has been shown to have numerous advantages for manufacturers. Comparatively low training time, real-time responsiveness to dynamical systems, data-driven decision logic, and the ability to quantify uncertainty are among the strongest benefits offered by PIML in contrast to physical methods. On the other hand, PIML's innate physical consistency is the primary benefit when compared with purely data-driven methods.

Future work in PIML for metal AM is envisioned to fall into two areas: general ML advancements and PIML-specific advancements. The first area includes topics such as ML model interpretability and cybersecurity that are important issues outside of a purely physics-informed paradigm. As for the second area, PIML must continuously incorporate state-of-the-art ML advances that address and resolve limitations inherent to ML as a whole to remain relevant. Otherwise, the benefits of PIML may be outweighed by the improved ML models that are computationally more powerful yet retaining the fundamental problems of lacking in physical interpretability. Additionally, as evidenced by Section 4.3, PIMI has been used much more than any other tenet of PIML at large. While understandable, since PIMI is the most convenient to implement of the five, the benefits of the remaining four are believed to be underexplored and underdeveloped at this time. Recent advancements such as PINN, WaveletKernelNet, and LRP have shown to be effective and foundational tools in advancing PIML. It is envisioned that they will receive increasing attention as PIMI becomes standard practice.

PIML data availability also remains an unsolved issue as does the development of ML architectures and components that are designed specifically for PIML. For instance, current CNN models learn image features through highly abstract convolution kernels that are learned through unconstrained optimization. The lack of constraints all but ensures that these maps have no physical relevance, thus moving away from PIML. If the learning process were to be constrained by physics such as by using a physics-regularized loss function or by tailoring the model architecture and components to be physics-adherent, then training the network would be synonymous with extracting physics-informed information from the data. While some forms of PIML are relatively simple to implement, e.g., PIMI, PIML mechanisms like that described above remain elusive. While the situation poses a continued challenge for manufacturers to improve productivity and quality, this situation also motivates researchers to redouble their efforts that produce the next generation machine learning algorithms that are smarter, faster, and physically transparent.

Declaration of Competing Interest

The authors report no declarations of interest.

Acknowledgments

C. Cooper acknowledges support provided by the National Science Foundation Graduate Research Fellowship under Grant No. 1937968. R. Gao and Y. Guo acknowledge support provided by the National Science Foundation under award No. CMMI-2040288/2040358. The authors thank Mr. J. Zhang at Case Western Reserve University for his helpful input in revising this paper.

References

[1] Gao C, Wolff S, Wang S. Eco-friendly additive manufacturing of metals: energy efficiency and life cycle analysis. J Manuf Syst 2021;60:459–72. https://doi.org/10.1016/j.jmsy.2021.06.011.
[2] Grasso M, Colosimo BM. Process defects and in situ monitoring methods in metal powder bed fusion: a review. Meas Sci Technol 2017;28(4):044005.
[3] Li C, Liu JF, Guo Y. Efficient multiscale prediction of cantilever distortion by selective laser melting. Proc. 27th Annu. Int. Solid Free. Fabr. Symp. 2016.
[4] Shi Q, Gu D, Xia M, Cao S, Rong T. Effects of laser processing parameters on thermal behavior and melting/solidification mechanism during selective laser melting of TiC/Inconel 718 composites. Opt Laser Technol 2016;84:9–22.
[5] Mitchell TM. Machine learning. New York: McGraw-hill; 1997.
[6] Wang YM, Voisin T, McKeown JT, Ye J, Calta NP, Li Z, et al. Additively manufactured hierarchical stainless steels with high strength and ductility. Nat Mater 2018;17(1):63–71.
[7] Voyant C, Notton G, Kalogirou S, Nivet M-L, Paoli C, Motte F, et al. Machine learning methods for solar radiation forecasting: a review. Renew Energy 2017;105:569–82.
[8] Johnson NS, Vulimiri PS, To AC, Zhang X, Brice CA, Kappes BB, et al. Invited review: machine learning for materials developments in metals additive manufacturing. Addit Manuf 2020;36:101641. https://doi.org/10.1016/j.addma.2020.101641.
[9] Tarsha-Kurdi F, Landes T, Grussenmeyer P, Koehl M. Model-driven and data-driven approaches using LIDAR data: analysis and comparison. 2007.
[10] Wang J, Chang Q, Xiao G, Wang N, Li S. Data driven production modeling and simulation of complex automobile general assembly plant. Comput Ind 2011;62(7):765–75.
[11] Pozdnoukhov A, Foresti L, Kanevski M. Data-driven topo-climatic mapping with machine learning methods. Nat Hazards 2009;50(3):497–518.
[12] Swischuk R, Mainini L, Peherstorfer B, Willcox K. Projection-based model reduction: formulations for physics-based machine learning. Comput Fluids 2019;179:704–17.
[13] Schlimmer JC, Granger RH. Incremental learning from noisy data. Mach Learn 1986;1(3):317–54.
[14] Moore JL, Dickson-Deane C, Galyen K. e-Learning, online learning, and distance learning environments: are they the same? Internet High Educ 2011;14(2):129–35.
[15] Chan SL, Lu Y, Wang Y. Data-driven cost estimation for additive manufacturing in cybermanufacturing. J Manuf Syst 2018;46:115–26. https://doi.org/10.1016/j.jmsy.2017.12.001.
[16] Zhang Y, Zhao YF. Hybrid sparse convolutional neural networks for predicting manufacturability of visual defects of laser powder bed fusion processes. J Manuf Syst 2021. https://doi.org/10.1016/j.jmsy.2021.07.002.
[17] Hertlein N, Buskohl PR, Gillman A, Vemaganti K, Anand S. Generative adversarial network for early-stage design flexibility in topology optimization for additive manufacturing. J Manuf Syst 2021;59:675–85. https://doi.org/10.1016/j.jmsy.2021.04.007.
[18] Liu C, Law ACC, Roberson D, Kong Z. Image analysis-based closed loop quality control for additive manufacturing with fused filament fabrication. J Manuf Syst 2019;51:75–86. https://doi.org/10.1016/j.jmsy.2019.04.002.
[19] Wang J, Ma Y, Zhang L, Gao RX, Wu D. Deep learning for smart manufacturing: methods and applications. J Manuf Syst 2018;48:144–56. https://doi.org/10.1016/j.jmsy.2018.01.003.
[20] Khanzadeh M, Chowdhury S, Marufuzzaman M, Tschopp MA, Bian L. Porosity prediction: supervised-learning of thermal history for direct laser deposition. J Manuf Syst 2018;47:69–82.

[21] Khanzadeh M, Chowdhury S, Tschopp MA, Doude HR, Marufuzzaman M, Bian L. In-situ monitoring of melt pool images for porosity prediction in directed energy deposition processes. IISE Trans 2019;51(5):437–55.
[22] Guo S, Guo WG, Bian L. Hierarchical spatial-temporal modeling and monitoring of melt pool evolution in laser-based additive manufacturing. IISE Trans 2020;52 (9):977–97. https://doi.org/10.1080/24725854.2019.1704465.
[23] Shevchik SA, Kenel C, Leinenbach C, Wasmer K. Acoustic emission for in situ quality monitoring in additive manufacturing using spectral convolutional neural networks. Addit Manuf 2018;21:598–604.
[24] Wasmer K, Le-Quang T, Meylan B, Shevchik S. In situ quality monitoring in AM using acoustic emission: a reinforcement learning approach. J Mater Eng Perform 2019;28(2):666–72.
[25] Jafari-Marandi R, Khanzadeh M, Tian W, Smith B, Bian L. From in-situ monitoring toward high-throughput process control: cost-driven decision-making framework for laser-based additive manufacturing. J Manuf Syst 2019;51:29–41. https://doi.org/10.1016/j.jmsy.2019.02.005.
[26] Liu C, Roux LL, Ji Z, Kerfriden P, Lacan F, Bigot S. Machine Learning-enabled feedback loops for metal powder bed fusion additive manufacturing. Procedia Comput Sci 2020;176:2586–95. https://doi.org/10.1016/j.procs.2020.09.314.
[27] Renken V, Albinger S, Goch G, Neef A, Emmelmann C. Development of an adaptive, self-learning control concept for an additive manufacturing process. CIRP J Manuf Sci Technol 2017;19:57–61. https://doi.org/10.1016/j.cirpj.2017.05.002.
[28] Sadoughi M, Hu C. Physics-based convolutional neural network for fault diagnosis of rolling element bearings. IEEE Sens J 2019;19(11):4181–92.
[29] Ball JE, Anderson DT, Chan CS. Comprehensive survey of deep learning in remote sensing: theories, tools, and challenges for the community. J Appl Remote Sens 2017;11(4):042609.
[30] Kouraytem N, Li X, Tan W, Kappes B, Spear AD. Modeling process–structure–property relationships in metal additive manufacturing: a review on physics-driven versus data-driven approaches. J Phys: Mater 2021;4 (3):032002. https://doi.org/10.1088/2515-7639/abca7b.
[31] Zhang Y, Wu L, Guo X, Kane S, Deng Y, Jung Y-G, et al. Additive manufacturing of metallic materials: a review. J Mater Eng Perform 2018;27(1):1–13. https://doi.org/10.1007/s11665-017-2747-y.
[32] Wang C, Tan XP, Tor SB, Lim CS. Machine learning in additive manufacturing: state-of-the-art and perspectives. Addit Manuf 2020;36:101538. https://doi.org/10.1016/j.addma.2020.101538.
[33] DebRoy T, Mukherjee T, Wei HL, Elmer JW, Milewski JO. Metallurgy, mechanistic models and machine learning in metal printing. Nat Rev Mater 2021; 6(1):48–68. https://doi.org/10.1038/s41578-020-00236-1.
[34] Kodama H. Automatic method for fabricating a three-dimensional plastic model with photo-hardening polymer. Rev Sci Instrum 1981;52(11):1770–3. https://doi.org/10.1063/1.1136492.
[35] Hull, CW, Apparatus for production of three-dimensional objects by stereolithography. United States Patent, Appl., No. 638905, Filed. (1984).
[36] ASTM52900-15 standard terminology for additive manufacturing—general Principles—terminology, vol. 3. West Conshohocken, PA: ASTM International; 2015 (4): p. 5.
[37] Brown, CO, Breinan, EM, Kear, BH, Method for fabricating articles by sequential layer deposition. (1982) Google Patents.
[38] Deckard, CR, Method and apparatus for producing parts by selective sintering. (1989) Google Patents.
[39] Larson, R, Method and device for producing three-dimensional bodies. (1998) Google Patents.
[40] Meiners, W, Wissenbach, K, Gasser, A, Shaped body especially prototype or replacement part production. DE Patent, 19. (1998).
[41] Griffith M, Keicher D, Atwood CL. Free form fabrication of metallic components using laser engineered net shaping (LENS {trademark}). Albuquerque, NM (United States): Sandia National Labs.; 1996.
[42] Stecker, S, Wollenhaupt, PE, Electron beam layer manufacturing using scanning electron monitored closed loop control. (2013) Google Patents.
[43] Wollenhaupt, PE, Stecker, S, Raster methodology, apparatus and system for electron beam layer manufacturing using closed loop control. (2013) Google Patents.
[44] King WE, Anderson AT, Ferencz RM, Hodge NE, Kamath C, Khairallah SA, et al. Laser powder bed fusion additive manufacturing of metals; physics, computational, and materials challenges. Appl Phys Rev 2015;2(4):041304. https://doi.org/10.1063/1.4937809.
[45] Sidambe AT. Biocompatibility of advanced manufactured titanium implants—a review. Materials 2014;7(12):8168–88.
[46] Gibson I, Rosen D, Stucker B. Powder bed fusion processes. In: Gibson I, Rosen D, Stucker B, editors. Additive manufacturing technologies: 3D printing, rapid prototyping, and direct digital manufacturing. New York, NY: Springer New York; 2015. p. 107–45.
[47] Lowther M, Louth S, Davey A, Hussain A, Ginestra P, Carter L, et al. Clinical, industrial, and research perspectives on powder bed fusion additively manufactured metal implants. Addit Manuf 2019;28:565–84. https://doi.org/10.1016/j.addma.2019.05.033.
[48] Dass A, Moridi A. State of the art in directed energy deposition: from additive manufacturing to materials design. Coatings 2019;9(7):418.
[49] Atwood C, Griffith M, Harwell L, Schlienger E, Ensz M, Smugeresky J, et al. Laser engineered net shaping (LENSTM): a tool for direct fabrication of metal parts. International congress on applications of lasers & electro-optics. Laser Institute of America; 1998.
[50] Bhatt PM, Malhan RK, Shembekar AV, Yoon YJ, Gupta SK. Expanding capabilities of additive manufacturing through use of robotics technologies: a survey. Addit Manuf 2020;31:100933. https://doi.org/10.1016/j.addma.2019.100933.
[51] Gibson I, Rosen D, Stucker B. Directed energy deposition processes. In: Gibson I, Rosen D, Stucker B, editors. Additive manufacturing technologies: 3D printing, rapid prototyping, and direct digital manufacturing. New York, NY: Springer New York; 2015. p. 245–68.
[52] Gradl, PR, Protz, CS, Zagorski, K, Doshi, V, McCallum, H, Additive manufacturing and hot-fire testing of bimetallic GRCop-84 and C-18150 channel-cooled combustion chambers using powder bed fusion and Inconel 625 hybrid directed energy deposition, In: AIAA propulsion and energy 2019 forum.
[53] DebRoy T, Wei H, Zuback J, Mukherjee T, Elmer J, Milewski J, et al. Additive manufacturing of metallic components–process, structure and properties. Prog Mater Sci 2018;92:112–224.
[54] Li C, White R, Fang X, Weaver M, Guo Y. Microstructure evolution characteristics of Inconel 625 alloy from selective laser melting to heat treatment. Mater Sci Eng A 2017;705:20–31.
[55] Li C, Guo Y, Zhao J. Interfacial phenomena and characteristics between the deposited material and substrate in selective laser melting Inconel 625. J Mater Process Technol 2017;243:269–81.
[56] Amato K, Hernandez J, Murr L, Martinez E, Gaytan S, Shindo P, et al. Comparison of microstructures and properties for a Ni-base superalloy (Alloy 625) fabricated by electron and laser beam melting. J Mater Sci Res 2012;1(2):3.
[57] Amato K, Gaytan S, Murr LE, Martinez E, Shindo P, Hernandez J, et al. Microstructures and mechanical behavior of Inconel 718 fabricated by selective laser melting. Acta Mater 2012;60(5):2229–39.
[58] Callister Jr WD, Rethwisch DG. Fundamentals of materials science and engineering: an integrated approach. John Wiley & Sons; 2020.
[59] Lewis GK, Schlienger E. Practical considerations and capabilities for laser assisted direct metal deposition. Mater Des 2000;21(4):417–23.
[60] Dadbakhsh S, Hao L, Sewell N. Effect of selective laser melting layout on the quality of stainless steel parts. Rapid Prototyp J 2012;18(3):241–9.
[61] Li R, Shi Y, Wang Z, Wang L, Liu J, Jiang W. Densification behavior of gas and water atomized 316L stainless steel powder during selective laser melting. Appl Surf Sci 2010;256(13):4350–6.
[62] Leuders S, Thöne M, Riemer A, Niendorf T, Tröster T, Richard HA, et al. On the mechanical behaviour of titanium alloy TiAl6V4 manufactured by selective laser melting: fatigue resistance and crack growth performance. Int J Fatigue 2013;48: 300–7.
[63] Khorasani AM, Yazdi MRS, Safizadeh MS. Analysis of machining parameters effects on surface roughness: a review. Int J Comput Mater Sci Surf Eng 2012;5 (1):68–84. https://doi.org/10.1504/IJCMSSE.2012.049055. 2021/06/23.
[64] Oberg E, Jones FD. Machinery's handbook, vol. 1916. Industrial press; 1916.
[65] Abe F. Direct manufacturing of metallic tools by laser rapid prototyping. Advanced technology of plasticity, proc. of the 6th ICTP 1999:1005–10.
[66] Abe F, Osakada K, Shiomi M, Uematsu K, Matsumoto M. The manufacturing of hard tools from metallic powders by selective laser melting. J Mater Process Technol 2001;111(1–3):210–3.
[67] Meiners W, Wissenbach K, Poprawe R. Direct generation of metal parts and tools by selective laser powder remelting (SLPR). International congress on applications of lasers & electro-optics. Laser Institute of America; 1998.
[68] Over C, Meiners W, Wissenbach K, Lindemann M, Hammann G. Selective laser melting: a new approach for the direct manufacturing of metal parts and tools. Proceedings of the international conferences on LANE 2001.
[69] Mazumder J, Schifferer A, Choi J. Direct materials deposition: designed macro and microstructure. Mater Res Innov 1999;3(3):118–31.
[70] Mazumder J, Dutta D, Kikuchi N, Ghosh A. Closed loop direct metal deposition: art to part. Opt Lasers Eng 2000;34(4–6):397–414.
[71] Resch M, Kaplan AF, Schuoecker D. Laser-assisted generating of three-dimensional parts by the blown powder process. XIII International symposium on gas flow and chemical lasers and high-power laser conference 2001. International Society for Optics and Photonics.
[72] Mirkoohi E, Mahdavi M, Li D, Garmestani H, Liang SY. Microstructure affected residual stress prediction based on mechanical threshold stress in direct metal deposition of Ti-6Al-4 V". Int J Adv Manuf Technol 2021;112(5):1705–12. https://doi.org/10.1007/s00170-020-06526-w.
[73] Deng D, Peng RL, Brodin H, Moverare J. Microstructure and mechanical properties of Inconel 718 produced by selective laser melting: sample orientation dependence and effects of post heat treatments. Mater Sci Eng A 2018;713: 294–306. https://doi.org/10.1016/j.msea.2017.12.043.
[74] Varotsis AB. 3D printing vs. CNC machining. Available from:. 2020. https://www.3dhubs.com/knowledge-base/3d-printing-vs-cnc-machining/.
[75] Pereira T, Kennedy JV, Potgieter J. A comparison of traditional manufacturing vs additive manufacturing, the best method for the job. Procedia Manuf 2019;30: 11–8. https://doi.org/10.1016/j.promfg.2019.02.003.
[76] Christodoulou L, Barnes J, Slattery K, Peels J, Rogers P. Comparison of additive manufacturing & CNC machining. Digital Alloys. 2019. https://www.digitalalloys.com/blog/comparison-additive-manufacturing-cnc-machining/.
[77] D., J. 3D Printing vs CNC Machining: which is best for prototyping?. Available from:. 2018. https://www.3dnatives.com/en/3d-printing-vs-cnc-160320184/#!.
[78] Hertlein N, Deshpande S, Venugopal V, Kumar M, Anand S. Prediction of selective laser melting part quality using hybrid Bayesian network. Addit Manuf 2020;32: 101089. https://doi.org/10.1016/j.addma.2020.101089.
[79] Aoyagi K, Wang H, Sudo H, Chiba A. Simple method to construct process maps for additive manufacturing using a support vector machine. Addit Manuf 2019;27: 353–62. https://doi.org/10.1016/j.addma.2019.03.013.

[80] Gardner JM, Hunt KA, Ebel AB, Rose ES, Zylich SC, Jensen BD, et al. Machines as craftsmen: localized parameter setting optimization for fused filament fabrication 3D printing. Adv Mater Technol 2019;4(3):1800653. https://doi.org/10.1002/admt.201800653.

[81] Wang T, Kwok T-H, Zhou C, Vader S. In-situ droplet inspection and closed-loop control system using machine learning for liquid metal jet printing. J Manuf Syst 2018;47:83–92. https://doi.org/10.1016/j.jmsy.2018.04.003.

[82] Khanzadeh M, Rao P, Jafari-Marandi R, Smith BK, Tschopp MA, Bian L. Quantifying geometric accuracy with unsupervised machine learning: using self-organizing map on fused filament fabrication additive manufacturing parts. J Manuf Sci Eng 2018;140(3).

[83] Marshall GJ, Thompson SM, Shamsaei N. Data indicating temperature response of Ti–6Al–4V thin-walled structure during its additive manufacture via Laser Engineered Net shaping. Data Brief 2016;7:697–703.

[84] Grasso M, Demir AG, Previtali B, Colosimo BM. In situ monitoring of selective laser melting of zinc powder via infrared imaging of the process plume. Robot Comput Integr Manuf 2018;49:229–39. https://doi.org/10.1016/j.rcim.2017.07.001.

[85] Gaikwad A, Yavari R, Montazeri M, Cole K, Bian L, Rao P. Toward the digital twin of additive manufacturing: Integrating thermal simulations, sensing, and analytics to detect process faults. IISE Trans 2020:1–14.

[86] Imani F, Gaikwad A, Montazeri M, Rao P, Yang H, Reutzel E. Process mapping and in-process monitoring of porosity in laser powder bed fusion using layerwise optical imaging. J Manuf Sci Eng 2018;140(10).

[87] Montazeri M, Nassar AR, Stutzman CB, Rao P. Heterogeneous sensor-based condition monitoring in directed energy deposition. Addit Manuf 2019;30:100916.

[88] Seifi SH, Tian W, Doude H, Tschopp MA, Bian L. Layer-wise modeling and anomaly detection for laser-based additive manufacturing. J Manuf Sci Eng 2019;141(8).

[89] Caggiano A, Zhang J, Alfieri V, Caiazzo F, Gao R, Teti R. Machine learning-based image processing for on-line defect recognition in additive manufacturing. CIRP Ann 2019;68(1):451–4.

[90] Guo S, Guo WG, Bain L. Hierarchical spatial-temporal modeling and monitoring of melt pool evolution in laser-based additive manufacturing. IISE Trans 2020;52(9):977–97. https://doi.org/10.1080/24725854.2019.1704465.

[91] Mahato V, Obeidi MA, Brabazon D, Cunningham P. Detecting voids in 3D printing using melt pool time series data. J Intell Manuf 2020. https://doi.org/10.1007/s10845-020-01694-8.

[92] Donegan SP, Schwalbach EJ, Groeber MA. Zoning additive manufacturing process histories using unsupervised machine learning. Mater Charact 2020;161:110123. https://doi.org/10.1016/j.matchar.2020.110123.

[93] Shevchik SA, Masinelli G, Kenel C, Leinenbach C, Wasmer K. Deep learning for in situ and real-time quality monitoring in additive manufacturing using acoustic emission. IEEE Trans Industr Inform 2019;15(9):5194–203.

[94] Zhang J, Wang P, Gao RX. Deep learning-based tensile strength prediction in fused deposition modeling. Comput Ind 2019;107:11–21.

[95] Montazeri M, Nassar AR, Dunbar AJ, Rao P. In-process monitoring of porosity in additive manufacturing using optical emission spectroscopy. IISE Trans 2020;52(5):500–15.

[96] Nguyen L, Buhl J, Bambach M. Continuous Eulerian tool path strategies for wire-arc additive manufacturing of rib-web structures with machine-learning-based adaptive void filling. Addit Manuf 2020;35:101265. https://doi.org/10.1016/j.addma.2020.101265.

[97] Okaro IA, Jayasinghe S, Sutcliffe C, Black K, Paoletti P, Green PL. Automatic fault detection for laser powder-bed fusion using semi-supervised machine learning. Addit Manuf 2019;27:42–53.

[98] Helm JM, Swiergosz AM, Haeberle HS, Karnuta JM, Schaffer JL, Krebs VE, et al. Machine learning and artificial intelligence: definitions, applications, and future directions. Curr Rev Musculoskelet Med 2020;13(1):69–76. https://doi.org/10.1007/s12178-020-09600-8.

[99] Ayodele TO. Types of machine learning algorithms. New advances in machine learning, vol. 3; 2010. p. 19–48.

[100] Dziugaite GK, Ben-David S, Roy DM. Enforcing interpretability and its statistical impacts: trade-offs between accuracy and interpretability. arXiv preprint arXiv:2010.13764. 2020.

[101] Zhu X, Goldberg AB. Introduction to semi-supervised learning. Synth Lect Artif Intell Mach Learn 2009;3(1):1–130.

[102] Xie X, Bennett J, Saha S, Lu Y, Cao J, Liu WK, et al. Mechanistic data-driven prediction of as-built mechanical properties in metal additive manufacturing. NPJ Comput Mater 2021;7(1):1–12.

[103] Li X, Siahpour S, Lee J, Wang Y, Shi J. Deep learning-based intelligent process monitoring of directed energy deposition in additive manufacturing with thermal images. Procedia Manuf 2020;48:643–9. https://doi.org/10.1016/j.promfg.2020.05.093.

[104] Russell S, Norvig P. Artificial intelligence: a modern approach. 3rd ed. Upp Saddle River: Prentice Hall; 2010.

[105] Sutton RS, Barto AG. Reinforcement learning: an introduction. MIT press; 2018.

[106] Ogoke F, Farimani AB. Thermal control of laser powder bed fusion using deep reinforcement learning. Addit Manuf 2021;46:102033. https://doi.org/10.1016/j.addma.2021.102033.

[107] Nian R, Liu J, Huang B. A review on reinforcement learning: introduction and applications in industrial process control. Comput Chem Eng 2020;139:106886. https://doi.org/10.1016/j.compchemeng.2020.106886.

[108] Wasmer K, Le-Quang T, Meylan B, Vakili-Farahani F, Olbinado MP, Rack A, et al. Laser processing quality monitoring by combining acoustic emission and machine learning: a high-speed X-ray imaging approach. Procedia CIRP 2018;74:654–8. https://doi.org/10.1016/j.procir.2018.08.054.

[109] Razaviarab N, Sharifi S, Banadaki YM. Smart additive manufacturing empowered by a closed-loop machine learning algorithm. Nano-, bio-, info-tech sensors and 3D systems III. International Society for Optics and Photonics; 2019.

[110] Zhang Y, Hong GS, Ye D, Zhu K, Fuh JYH. Extraction and evaluation of melt pool, plume and spatter information for powder-bed fusion AM process monitoring. Mater Des 2018;156:458–69. https://doi.org/10.1016/j.matdes.2018.07.002.

[111] Snow Z, Diehl B, Reutzel EW, Nassar A. Toward in-situ flaw detection in laser powder bed fusion additive manufacturing through layerwise imagery and machine learning. J Manuf Syst 2021;59:12–26. https://doi.org/10.1016/j.jmsy.2021.01.008.

[112] Ye D, Hsi Fuh JY, Zhang Y, Hong GS, Zhu K. In situ monitoring of selective laser melting using plume and spatter signatures by deep belief networks. ISA Trans 2018;81:96–104. https://doi.org/10.1016/j.isatra.2018.07.021.

[113] Imani F, Chen R, Diewald E, Reutzel E, Yang H. Deep learning of variant geometry in layerwise imaging profiles for additive manufacturing quality control. J Manuf Sci Eng 2019;141(11).

[114] Gobert C, Reutzel EW, Petrich J, Nassar AR, Phoha S. Application of supervised machine learning for defect detection during metallic powder bed fusion additive manufacturing using high resolution imaging. Addit Manuf 2018;21:517–28.

[115] Gawade V, Singh V, Guo WG. Leveraging simulated and empirical data-driven insight to supervised-learning for porosity prediction in laser metal deposition. J Manuf Syst 2021. https://doi.org/10.1016/j.jmsy.2021.07.013.

[116] Mojahed Yazdi R, Imani F, Yang H. A hybrid deep learning model of process-build interactions in additive manufacturing. J Manuf Syst 2020;57:460–8. https://doi.org/10.1016/j.jmsy.2020.11.001.

[117] Scime L, Beuth J. Using machine learning to identify in-situ melt pool signatures indicative of flaw formation in a laser powder bed fusion additive manufacturing process. Addit Manuf 2019;25:151–65.

[118] Scime L, Beuth J. A multi-scale convolutional neural network for autonomous anomaly detection and classification in a laser powder bed fusion additive manufacturing process. Addit Manuf 2018;24:273–86.

[119] Scime L, Beuth J. Anomaly detection and classification in a laser powder bed additive manufacturing process using a trained computer vision algorithm. Addit Manuf 2018;19:114–26.

[120] Chen L, Yao X, Xu P, Moon SK, Bi G. Rapid surface defect identification for additive manufacturing with in-situ point cloud processing and machine learning. Virtual Phys Prototyp 2021;16(1):50–67. https://doi.org/10.1080/17452759.2020.1832695.

[121] Li X, Jia X, Yang Q, Lee J. Quality analysis in metal additive manufacturing with deep learning. J Intell Manuf 2020;31(8):2003–17. https://doi.org/10.1007/s10845-020-01549-2.

[122] Kunkel MH, Gebhardt A, Mpofu K, Kallweit S. Quality assurance in metal powder bed fusion via deep-learning-based image classification. Rapid Prototyp J 2019;26(2):259–66.

[123] Desai PS, Higgs CF. Spreading process maps for powder-bed additive manufacturing derived from physics model-based machine learning. Metals 2019;9(11):1176.

[124] Kappes B, Moorthy S, Drake D, Geerlings H, Stebner A. Machine learning to optimize additive manufacturing parameters for laser powder bed fusion of Inconel 718. Proceedings of the 9th International Symposium on Superalloy 718 & Derivatives: Energy, Aerospace, and Industrial Applications 2018. Springer.

[125] Caiazzo F, Caggiano A. Laser Direct Metal Deposition of 2024 Al alloy: trace geometry prediction via machine learning. Materials 2018;11(3):444.

[126] Gaikwad A, Imani F, Rao P, Yang H, Reutzel E. Design rules and in-situ quality monitoring of thin-wall features made using laser powder bed fusion. International manufacturing science and engineering conference 2019. American Society of Mechanical Engineers.

[127] Francis J, Bian L. Deep learning for distortion prediction in laser-based additive manufacturing using big data. Manuf Lett 2019;20:10–4. https://doi.org/10.1016/j.mfglet.2019.02.001.

[128] Lee S, Peng J, Shin D, Choi YS. Data analytics approach for melt-pool geometries in metal additive manufacturing. Sci Technol Adv Mater 2019;20(1):972–8. https://doi.org/10.1080/14686996.2019.1671140.

[129] Xia C, Pan Z, Polden J, Li H, Xu Y, Chen S. Modelling and prediction of surface roughness in wire arc additive manufacturing using machine learning. J Intell Manuf 2021. https://doi.org/10.1007/s10845-020-01725-4.

[130] Akhil V, Raghav G, Arunachalam N, Srinivas DS. Image data-based surface texture characterization and prediction using machine learning approaches for additive manufacturing. J Comput Inf Sci Eng 2020;20(2). https://doi.org/10.1115/1.4045719. 6/24/2021.

[131] Xie X, Bennett J, Saha S, Lu Y, Cao J, Liu WK, et al. Mechanistic data-driven prediction of as-built mechanical properties in metal additive manufacturing. NPJ Comput Mater 2021;7(1):86. https://doi.org/10.1038/s41524-021-00555-z.

[132] Yan F, Chan Y-C, Saboo A, Shah J, Olson GB, Chen W. Data-driven prediction of mechanical properties in support of rapid certification of additively manufactured alloys. Comput Model Eng Sci 2018;117(3):343–66.

[133] Hassanin H, Alkendi Y, Elsayed M, Essa K, Zweiri Y. Controlling the properties of additively manufactured cellular structures using machine learning approaches. Adv Eng Mater 2020;22(3):1901338.

[134] Zhang M, Sun C-N, Zhang X, Goh PC, Wei J, Hardacre D, et al. High cycle fatigue life prediction of laser additive manufactured stainless steel: a machine learning approach. Int J Fatigue 2019;128:105194.

[135] Bennett J, Glerum J, Cao J. Relating additively manufactured part tensile properties to thermal metrics. CIRP Ann 2021;70(1):187–90. https://doi.org/10.1016/j.cirp.2021.04.053.

[136] Liu R, Liu S, Zhang X. A physics-informed machine learning model for porosity analysis in laser powder bed fusion additive manufacturing. Int J Adv Manuf Technol 2021;113(7):1943–58. https://doi.org/10.1007/s00170-021-06640-3.

[137] Mycroft W, Katzman M, Tammas-Williams S, Hernandez-Nava E, Panoutsos G, Todd I, et al. A data-driven approach for predicting printability in metal additive manufacturing processes. J Intell Manuf 2020:1–13.

[138] Karpatne A, Watkins W, Read J, Kumar V. Physics-guided neural networks (pgnn): an application in lake temperature modeling. arXiv preprint arXiv:1710.11431. 2017.

[139] Howland MF, Dabiri JO. Wind farm modeling with interpretable physics-informed machine learning. Energies 2019;12(14):2716.

[140] Li T, Zhao Z, Sun C, Cheng L, Chen X, Yan R, et al. WaveletKernelNet: an interpretable deep neural network for industrial intelligent diagnosis. IEEE Trans Syst Man Cybern Syst 2021:1–11. https://doi.org/10.1109/TSMC.2020.3048950.

[141] Yan R, Gao RX. Base wavelet selection for bearing vibration signal analysis. Int J Wavelets Multiresolut Inf Process 2009;07(04):411–26. https://doi.org/10.1142/s0219691309002994.

[142] Bach S, Binder A, Montavon G, Klauschen F, Müller K-R, Samek W. On pixel-wise explanations for non-linear classifier decisions by layer-wise relevance propagation. PLoS One 2015;10(7):e0130140.

[143] Ribeiro MT, Singh S, Guestrin C. "Why should I trust you?": Explaining the predictions of any classifier. Proceedings of the 22nd ACM SIGKDD international conference on knowledge discovery and data mining 2016:1135–44. Association for Computing Machinery: San Francisco, California, USA.

[144] Lundberg SM, Lee S-I. A unified approach to interpreting model predictions. Proceedings of the 31st international conference on neural information processing systems 2017.

[145] Grezmak J, Zhang J, Wang P, Loparo KA, Gao RX. Interpretable convolutional neural network through layer-wise relevance propagation for machine fault diagnosis. IEEE Sens J 2020;20(6):3172–81. https://doi.org/10.1109/JSEN.2019.2958787.

[146] Raissi M, Perdikaris P, Karniadakis GE. Physics-informed neural networks: a deep learning framework for solving forward and inverse problems involving nonlinear partial differential equations. J Comput Phys 2019;378:686–707.

[147] Long Z, Lu Y, Dong B. PDE-Net 2.0: learning PDEs from data with a numeric-symbolic hybrid deep network. J Comput Phys 2019;399:108925. https://doi.org/10.1016/j.jcp.2019.108925.

[148] Yang L, Zhang D, Karniadakis GE. Physics-informed generative adversarial networks for stochastic differential equations. SIAM J Sci Comput 2020;42(1):A292–317. https://doi.org/10.1137/18M1225409. 2021/10/01.

[149] Kim B, Azevedo VC, Thuerey N, Kim T, Gross M, Solenthaler B. Deep fluids: a generative network for parameterized fluid simulations. Comput Graph Forum 2019;38(2):59–70. https://doi.org/10.1111/cgf.13619. 2021/06/23.

[150] Stewart R, Ermon S. Label-free supervision of neural networks with physics and domain knowledge. Proceedings of the AAAI Conference on Artificial Intelligence 2017.

[151] Liu Z, Guo Y. A hybrid approach to integrate machine learning and process mechanics for the prediction of specific cutting energy. CIRP Ann 2018;67(1):57–60. https://doi.org/10.1016/j.cirp.2018.03.015.

[152] Karandikar J, Schmitz T, Smith S. Physics-guided logistic classification for tool life modeling and process parameter optimization in machining. J Manuf Syst 2021;59:522–34. https://doi.org/10.1016/j.jmsy.2021.03.025.

[153] Wang J, Li Y, Zhao R, Gao RX. Physics guided neural network for machining tool wear prediction. J Manuf Syst 2020;57:298–310. https://doi.org/10.1016/j.jmsy.2020.09.005.

[154] Greis NP, Nogueira ML, Bhattacharya S, Schmitz T. Physics-guided machine learning for self-aware machining. AAAI spring symposium–AI and manufacturing 2020.

[155] Zhang X, Wang Z, Liu D, Ling Q. Dada: deep adversarial data augmentation for extremely low data regime classification. In: ICASSP 2019–2019 IEEE international conference on acoustics, speech and signal processing (ICASSP); 2019.

[156] Herriott C, Spear AD. Predicting microstructure-dependent mechanical properties in additively manufactured metals with machine- and deep-learning methods. Comput Mater Sci 2020;175:109599. https://doi.org/10.1016/j.commatsci.2020.109599.

[157] Guo W, Tian Q, Guo S, Guo Y. A physics-driven deep learning model for process-porosity causal relationship and porosity prediction with interpretability in laser metal deposition. CIRP Ann - Manuf Technol 2020;69(1). https://doi.org/10.1016/j.cirp.2020.04.049.

[158] Kabir HMD, Khosravi A, Hosen MA, Nahavandi S. Neural network-based uncertainty quantification: a survey of methodologies and applications. IEEE Access 2018;6:36218–34. https://doi.org/10.1109/ACCESS.2018.2836917.

[159] Ren K, Chew Y, Zhang Y, Fuh J, Bi G. Thermal field prediction for laser scanning paths in laser aided additive manufacturing by physics-based machine learning. Comput Methods Appl Mech Eng 2020;362:112734.

[160] Nagarajan HP, Mokhtarian H, Jafarian H, Dimassi S, Bakrani-Balani S, Hamedi A, et al. Knowledge-based design of artificial neural network topology for additive manufacturing process modeling: a new approach and case study for fused deposition modeling. J Mech Des 2019;141(2).

[161] Zhu Q, Liu Z, Yan J. Machine learning for metal additive manufacturing: predicting temperature and melt pool fluid dynamics using physics-informed neural networks. Comput Mech 2021;67(2):619–35. https://doi.org/10.1007/s00466-020-01952-9.

[162] Paulson NH, Gould B, Wolff SJ, Stan M, Greco AC. Correlations between thermal history and keyhole porosity in laser powder bed fusion. Addit Manuf 2020;34:101213. https://doi.org/10.1016/j.addma.2020.101213.

[163] Finkbeiner M, Inaba A, Tan R, Christiansen K, Klüppel H-J. The new international standards for life cycle assessment: ISO 14040 and ISO 14044. Int J Life Cycle Assess 2006;11(2):80–5. https://doi.org/10.1065/lca2006.02.002.

[164] Wehmeyer C, Noé F. Time-lagged autoencoders: deep learning of slow collective variables for molecular kinetics. J Chem Phys 2018;148(24):241703.

[165] Roca JB, Vaishnav P, Fuchs ER, Morgan MG. Policy needed for additive manufacturing. Nat Mater 2016;15(8):815–8.

[166] Teng C, Gong H, Szabo A, Dilip JJS, Ashby K, Zhang S, et al. Simulating melt pool shape and lack of fusion porosity for selective laser melting of cobalt chromium components. J Manuf Sci Eng 2016;139(1):011009. https://doi.org/10.1115/1.4034137 (11 pages). 3/17/2021.

[167] Foroozmehr A, Badrossamay M, Foroozmehr E, Golabi Si. Finite element simulation of selective laser melting process considering optical penetration depth of laser in powder bed. Mater Des 2016;89:255–63. https://doi.org/10.1016/j.matdes.2015.10.002.

[168] Zou S, Xiao H, Ye F, Li Z, Tang W, Zhu F, et al. Numerical analysis of the effect of the scan strategy on the residual stress in the multi-laser selective laser melting. Results Phys 2020;16:103005. https://doi.org/10.1016/j.rinp.2020.103005.

[169] Rubinstein RY, Kroese DP. Simulation and the Monte Carlo method, vol. 10. John Wiley & Sons; 2016.

[170] Shorten C, Khoshgoftaar TM. A survey on image data augmentation for deep learning. J Big Data 2019;6(1):60.

[171] Frid-Adar M, Diamant I, Klang E, Amitai M, Goldberger J, Greenspan H. GAN-based synthetic medical image augmentation for increased CNN performance in liver lesion classification. Neurocomputing 2018;321:321–31.

[172] Chawla NV, Bowyer KW, Hall LO, Kegelmeyer WP. SMOTE: synthetic minority over-sampling technique. J Artif Intell Res 2002;16:321–57.

[173] Wang Y, Yao Q, Kwok JT, Ni LM. Generalizing from a few examples: a survey on few-shot learning. ACM Comput Surv 2020;53(3):1–34. https://doi.org/10.1145/3386252. 63.

[174] Bromley J, Bentz JW, Bottou L, Guyon I, Lecun Y, Moore C, et al. Signature verification using a "SIAMESE" time delay neural network. Intern J Pattern Recognit Artif Intell 1993;07(04):669–88. https://doi.org/10.1142/S0218001493000339. 2021/10/01.

[175] Hoffer E, Ailon N. Deep metric learning using triplet network. Similarity-based pattern recognition. Cham: Springer International Publishing; 2015.

[176] Liu FT, Ting KM, Zhou Z. Isolation Forest. 2008 Eighth IEEE international conference on data mining 2008.

[177] Yao JT, Vasilakos AV, Pedrycz W. Granular computing: perspectives and challenges. IEEE Trans Cybern 2013;43(6):1977–89. https://doi.org/10.1109/TSMCC.2012.2236648.

[178] Zhang J, Gao RX. Deep learning-driven data curation and model interpretation for smart manufacturing. Chin J Mech Eng 2021;34(1):71. https://doi.org/10.1186/s10033-021-00587-y.

[179] Dilip JJS, Zhang S, Teng C, Zeng K, Robinson C, Pal D, et al. Influence of processing parameters on the evolution of melt pool, porosity, and microstructures in Ti-6Al-4V alloy parts fabricated by selective laser melting. Prog Addit Manuf 2017;2(3):157–67. https://doi.org/10.1007/s40964-017-0030-2.

[180] Tian Q, Guo S, Melder E, Bian L, Guo WG. Deep learning-based data fusion method for in situ porosity detection in laser-based additive manufacturing. J Manuf Sci Eng 2020;143(4). https://doi.org/10.1115/1.4048957. 6/24/2021.

[181] Mello FLd. A survey on machine learning adversarial attacks. J Inf Secur Cryptogr (Enigma) 2020;7(1):1–7. https://doi.org/10.17648/jisc.v7i1.76.

[182] Brendel W, Rauber J, Bethge M. Decision-based adversarial attacks: reliable attacks against black-box machine learning models. arXiv preprint arXiv:1712.04248. 2017.

[183] Madry A, Makelov A, Schmidt L, Tsipras D, Vladu A. Towards deep learning models resistant to adversarial attacks. International conference on learning representations 2018.

[184] Madry A, Makelov A, Schmidt L, Tsipras D, Vladu A. Towards deep learning models resistant to adversarial attacks. arXiv preprint arXiv:1706.06083. 2017.

[185] Anthi E, Williams L, Rhode M, Burnap P, Wedgbury A. Adversarial attacks on machine learning cybersecurity defences in Industrial Control Systems. J Inf Secur Appl 2021;58:102717. https://doi.org/10.1016/j.jisa.2020.102717.

[186] Chakraborty A, Alam M, Dey V, Chattopadhyay A, Mukhopadhyay D. A survey on adversarial attacks and defences. CAAI Trans Intell Technol 2021;6(1):25–45. https://doi.org/10.1049/cit2.12028. 2021/06/24.

[187] Pal D, Patil N, Zeng K, Stucker B. An integrated approach to additive manufacturing simulations using physics based, coupled multiscale process modeling. J Manuf Sci Eng 2014;136(6).

[188] Sirignano J, Spiliopoulos K. DGM: a deep learning algorithm for solving partial differential equations. J Comput Phys 2018;375:1339–64.

[189] Yeo K, Melnyk I. Deep learning algorithm for data-driven simulation of noisy dynamical system. J Comput Phys 2019;376:1212–31.
[190] Nabian MA, Meidani H. Physics-driven regularization of deep neural networks for enhanced engineering design and analysis. J Comput Inf Sci Eng 2020;20(1).
[191] Kilkenny MF, Robinson KM. Data quality: "garbage in – garbage out". Health Inf Manag J 2018;47(3):103–5. https://doi.org/10.1177/1833358318774357. 2021/10/01.
[192] Zheng S, Song Y, Leung T, Goodfellow I. Improving the robustness of deep neural networks via stability training. Proceedings of the IEEE conference on computer vision and pattern recognition 2016.
[193] Malakooti B. Operations and production systems with multiple objectives. John Wiley & Sons; 2014.